Pool Boiling Enhancement Through Improved Liquid Supply Pathways Over Open Microchannels

by

Arvind Jaikumar

A Thesis Submitted in Partial Fulfillment of the Requirements for the Degree of Master of Science in Mechanical Engineering

Approved By:

Dr. Satish G. Kandlikar
Department of Mechanical Engineering _____
(Thesis Advisor)

Dr. Michael Schertzer
Department of Mechanical Engineering _____
(Examiner)

Dr. Surendra Gupta
Department of Mechanical Engineering _____
(Examiner)

Dr. Agamemnon Crassidis
Department of Mechanical Engineering _____
(Department representative)

Rochester Institute of Technology

Rochester, New York 14623

November 2014

Pool Boiling Enhancement Through Improved Liquid Supply Pathways Over Open Microchannels

by

Arvind Jaikumar

A Thesis Submitted in Partial Fulfillment of the Requirements for the Degree of Master of Science in Mechanical Engineering

Department of Mechanical Engineering
Kate Gleason College of Engineering

Rochester Institute of Technology

Rochester, New York 14623

November 2014

Acknowledgements

I would like to express my sincere gratitude to Dr. Satish Kandlikar for providing me the opportunity to pursue research in his globally recognized Thermal Analysis, Microfluidics and Fuel Cell laboratory. His support and guidance enabled me to understand the subject and also convinced me to pursue my PhD. Without his guidance and persistent help this dissertation would not have been possible.

I would also like to thank Dr. Surendra Gupta for his assistance in the study. I benefited immensely from his systematic approach to problem solving. As his teaching assistant, I benefitted from his teaching skills which I try to incorporate in every walk of life. Dr. Michael Schertzer has been very influential in the success of this work. His constant insights into the work helped me look at the study from a different perspective. Dr. Agamemnon Crassidis was my first acquaintance at RIT. His continual support during the course of my study significantly helped me.

This thesis would not be complete without thanking Robert Kraynik, Jan Maneti, David Hathaway, Alyssa Recinella and Brittany Klimtzak for their help in fabricating the test surfaces. I would also like to thank my lab members for their constant support in helping me complete my thesis.

Education in my family was something that was akin to religious devotion (My father is a Mechanical Engineering graduate, post-graduate in Material Science from Indian Institute of Technology- Mumbai and is presently working as a Scientist with Defense Research & Development Organization) and hence at a very young age I developed the love and respect for knowledge that has been the cornerstone of my life till

date. Their never ending support has bolstered my will to excel in my life. The confidence they instilled in me propelled my path to become a proficient engineer.

Abstract:

Boiling is an efficacious mode of heat transfer and is utilized in various energy conversions, heat exchange systems and in cooling of high energy density electronic components. Fundamental pool boiling mechanisms suggest that liquid rewetting on a heated surface is a key factor in delaying critical heat flux (CHF) for enhancing pool boiling performance. In this study, pool boiling enhancement is achieved by providing improved liquid supply pathways to nucleation sites in open microchannels.

A two part study is conducted to enhance pool boiling performance of open microchannels. Micromachined and porous surfaces are identified as enhancement techniques in Part-I and Part-II respectively. The results obtained in part-I showed significant improvement in the pool boiling performance when tested with water and FC-87. In part-II of the study, porous coatings are deposited on the boiling surface of an open parallel microchannel fin tops, channel bottoms and both, and individually investigated for their pool boiling performance. The best performing surface was with porous coatings throughout the geometry and had a CHF of 313 W/cm^2 at a wall superheat of 7.5 °C. High speed images for the three surfaces show that bubble nucleation occurred at the location of porous deposits. Furthermore, additional nucleation sites are identified as the main contributing factor in the best performing surface which had an enhancement of 150% in CHF when compared to a plain surface. Efficient liquid recirculation provided by open microchannels also contributed to improved microconvection in the channels.

Contents

List of figures

List of tables

Nomenclature

Saturation pressure	P_{sat}
Saturation temperature	T_{sat}
Latent heat of vaporization	h_{lv}
Density of liquid	ρ_l
Density of vapor	ρ_v
Dynamic viscosity of liquid	μ_l
Dynamic viscosity of vapor	μ_v
Thermal conductivity of liquid	k_l
Thermal conductivity of vapor	k_v
Surface tension	σ
Specific heat of liquid	$c_{p,l}$
Specific heat of vapor	$c_{p,v}$
Thermal diffusivity	α
Specific volume of vapor	ν_v
Specific volume of liquid	ν_l
Receding contact angle	θ_r
Heater surface temperature	T_s
Wall superheat	$\Delta T_{sat}=T_{wall}-T_{sat}$
Heat flux per unit area	q"
Heat transfer coefficient	h

Chapter 1

This chapter provides the background and motivation for the research study, and a detailed description of the boiling curve and bubble nucleation phenomenon in boiling.

1.1 Introduction:

Efficient cooling systems are of keen interest in many engineering applications. As the scale of the flow passages becomes small, the transport phenomenon becomes significant in these passages due to increase in area/volume ratio as well as more efficient heat transfer. Significant research in this field started after their first successful application in electronics cooling by Tuckerman and Pease [1] . Failure to cool devices adequately can lead to improper operation and material degradation. The two primary cooling schemes employed are air cooling and liquid cooling. Cooling methods can be achieved by two means, namely natural convection and forced convection. Fig. 1 shows the typical range of heat transfer coefficients for single phase and two phase cooling regimes for air and water. From the figure it is evident that two phase cooling is required for high heat dissipation rates due to high heat transfer coefficients to meet the demands of electronics cooling.

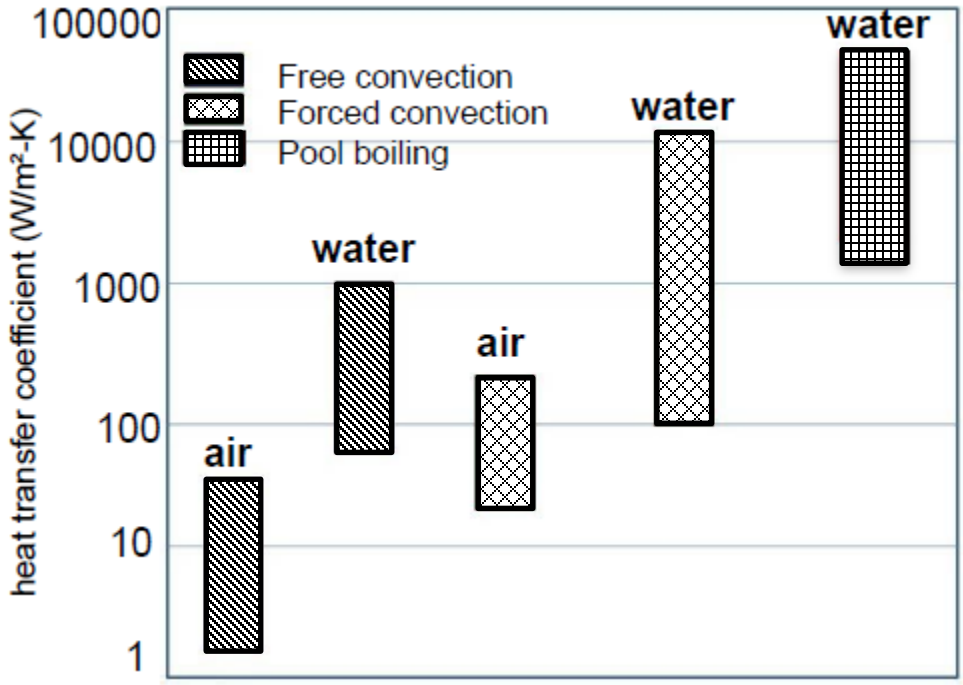

Figure 1. Typical values of heat transfer coefficients

Pool boiling is the phase change from liquid to vapor accompanied with bubble nucleation, growth and departure in a quiescent liquid where fluid motion is due to free convection. Pool boiling enhancement can be achieved by two methods namely (a) passive methods, (b) active methods. Passive methods are achieved by structured heat transfer surface without using external power whereas active methods involve using external power. Passive pool boiling heat transfer enhancement offers attractive cooling schemes in high power electronic systems and core of nuclear reactors. This technique does not require any moving parts, and is highly beneficial from both thermal and cost perspectives. The present miniaturization trend in microelectronic devices demands effective thermal management. Pool boiling has served as an efficacious means to dissipate large heat flux over a small footprint which has led to development of enhanced heat transfer surfaces. The main objective of these augmented surfaces is to reduce wall

superheat and increase critical heat flux which offers enhanced performance over a wide operating range. A typical pool boiling performance is characterized by the plot of heat flux versus wall superheat. The degree by which the curve shifts to the left and also higher Critical Heat Flux (CHF) value depicts the extent of enhancement compared to a flat surface.

1.2 Boiling curve:

The regimes of pool boiling are understood by plotting a curve of heat flux (q'') versus wall superheat (ΔT). Figure 2 shows a typical pool boiling curve with its four regimes.

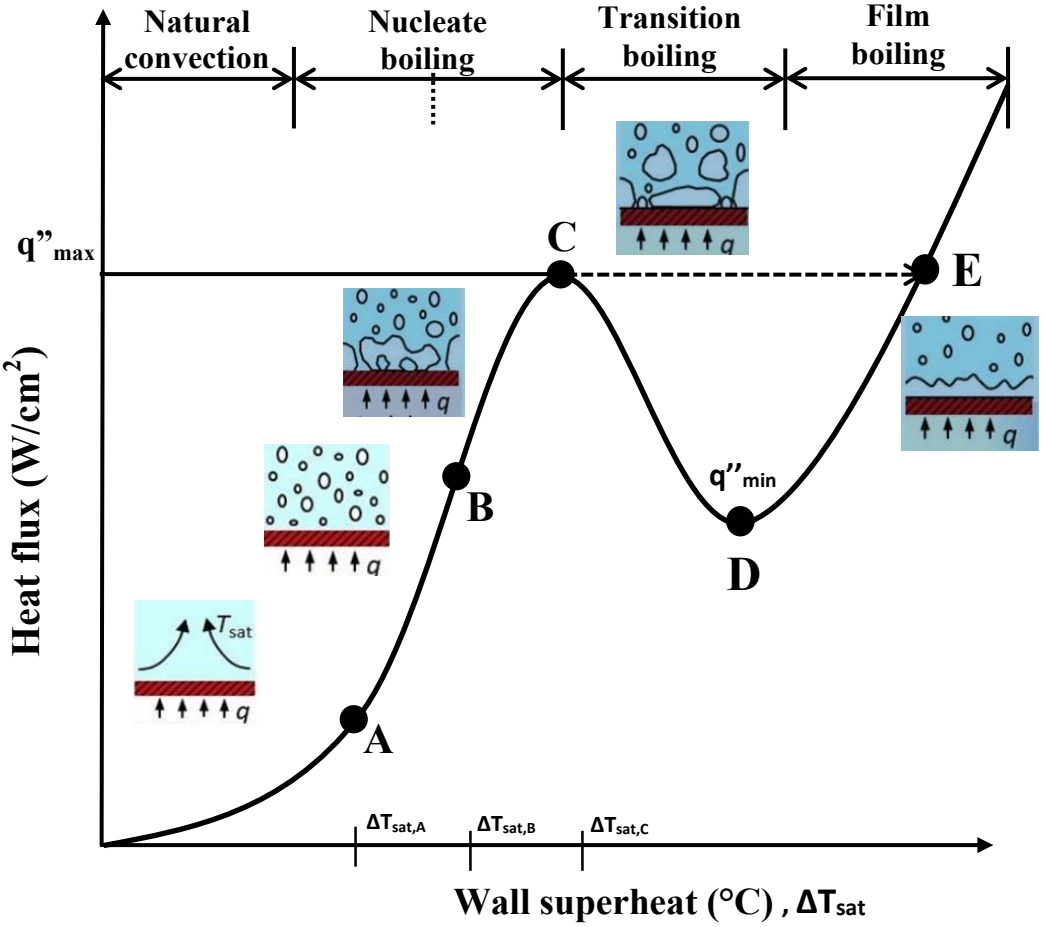

Figure 2. Pool boiling curve showing different regimes

The four regimes in pool boiling are described in the following section.

1.2.1 Free convection zone

When surface temperature (T_{wall}) is greater than the saturation temperature of water (T_{sat}), density of the fluid at the surface decreases. These result in hot fluid moving up and cold fluid moving down setting up natural convective currents. Thus, heat is transferred from the heated surface to water via free convection. It exists in the range

$\Delta T_{sat} < \Delta T_{sat,A}$. Where, $\Delta T_{sat,A}$ is referred to as Onset of nucleate boiling where the first bubble nucleates.

1.2.2 Nucleate boiling

Nucleate boiling is accompanied by nucleation and subsequent departure of bubbles on the heated surface. There are two distinguishable flow regimes in this region. This is shown as region A-C in Fig. 2. Firstly, in the region A-B , isolated bubbles form and get detached from the surface. This disturbance (separation) induces good fluid mixing increasing the heat transfer coefficient, 'h' and with an increase in the heat flux, 'q'''. Secondly, as the wall superheat ΔT_{sat} increases beyond a certain value indicated by $\Delta T_{sat,B}$ more nucleation sites become active and increased bubble formation causes bubble interference and coalescence. In the region B-C, bubbles coalesce and escape as jets or columns. Interference between these densely populated bubbles significantly reduces fluid motion at the heater surface. Point B corresponds to the point at which h is maximum. As ΔT_{sat} is increased further h starts to decrease although 'q''' continues to increase. This can be explained from the principle governing convection heat transfer equation, $q = hA(T_{wall} - T_{sat})$. As, $\Delta T_{sat} > \Delta T_{sat,B}$ the relative increase in ΔT_{sat} exceeds the reduction in h. At point C, called the Critical heat flux, increase in ΔT_{sat} is balanced by the decrease in h.

1.2.3 Transition boiling

This region exists in $\Delta T_{sat,C} <= \Delta T_{sat} <= \Delta T_{sat,D}$. The heat flux rate in nucleate boiling is very high as a result of agitating motion of bubbles. This intense formation of bubbles results in unstable film. This film has a very low thermal conductivity as it is formed by

vapor. The heat flux rate and ΔT_{sat} continues to increase as long as the agitating motion of bubbles overcomes the effects of the film. However, when the insulating effects of the film dominates the bubble agitation the heat flux rate decreases with increasing ΔT_{sat}. In this region, the conditions oscillate between film and nucleate boiling, i.e. the film is continually forming, collapsing and reforming. Since the thermal conductivity of the film is very low compared to that of the liquid, h and q_s must decrease with increasing ΔT_{sat}.

1.2.4 Film boiling

It exists in the region $\Delta T_{sat} > \Delta T_{sat,D}$ The surface is completely covered by vapor film. Point D is called the Leidenfrost point where the heat flux is minimum, $q''_{min.}$ Heat transfer from the heater surface to the liquid occurs by conduction in which water droplets falling on the hot liquid surface get separated from it by the film before eventually boiling away. As T_{wall} is increased heat flux increases as h increases. Then radiation effects take over resulting in heat flux rapidly increasing with increasing $\Delta T_{sat.}$

With the heat transfer being impeded due to a layer of vapor blanket in film and transition boiling, nucleate boiling is identified as the best region to dissipate high heat fluxes.

1.3 Bubble nucleation

Pool boiling situation consists of a heated surface at a higher temperature compared to the saturation temperature of the fluid boiling over it. For bubbles to form, certain conditions must be met. Entrapped gases facilitate growth of the bubble if the saturation temperature of the liquid surrounding the vapor bubble is greater than the temperature corresponding to the saturation pressure of the vapor. Fig 3 shows the different forces

acting on a bubble. The two forces for static bubble are surface tension and pressure forces due to liquid and vapor.

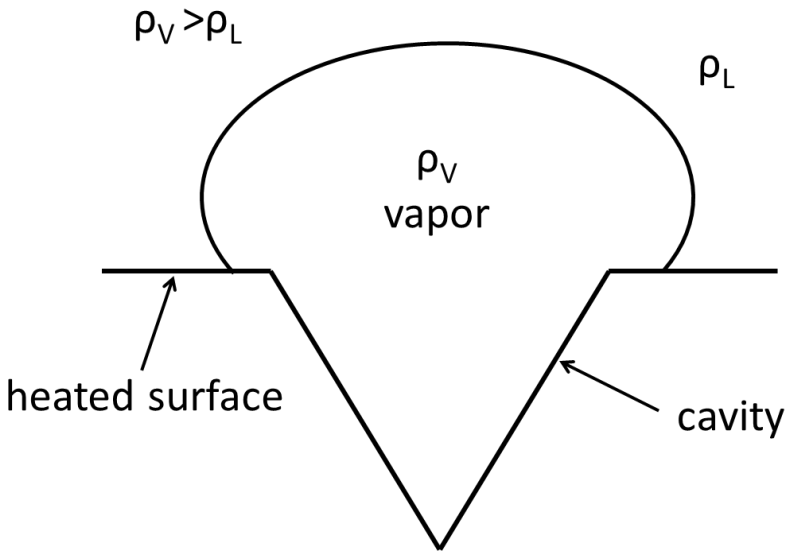

Figure 3. Bubble nucleation

The force balance is as shown below,

$$\pi R^2(\rho_V - \rho_l) - 2\pi R\sigma = 0 \quad (1)$$

From the above equation, vapor pressure can be represented as,

$$\rho_V = \rho_l + \frac{2\sigma}{R} \quad (2)$$

Equation (2) shows the dependence of bubble radius on the vapor pressure. For a small bubble, the vapor pressure is high indicating that saturation temperature will be higher for a fluid at pressure, ρ_V proving that a wall superheat is required.

The onset of nucleate boiling is characterized by a range of active nucleation sites proposed by Hsu and Graham [2] and Hsu [3] . Kandlikar and Spiesman [4] through simulations identified the thermal boundary thickness to be equal to 1.1R and modified

the equation proposed by Hsu [3]. Kandlikar et al. [5] further modified this equation by incorporating the effects of contact angle (receding) as shown below,

$$\{r_{cmax}, r_{cmin}\} = \frac{\delta_t \sin\theta_r}{2.2}\left(\frac{\Delta T_{sat}}{\Delta T_{sat} + \Delta T_{sub}}\right)\left[1 \pm \sqrt{1} - \frac{8.8\sigma T_{sat}\,(\Delta T_{sat} + \Delta T_{sub})}{\rho_V h_{lv} \delta_t {T_{sat}}^2}\right] \quad (3)$$

The bubble nucleation will occur if the radii lie within the range specified by Eq. (3). For a smooth polished surface, higher superheats are expected to initiate nucleation. The wall superheat is given by,

$$\Delta T_{sat,ONB\ at\ r_c} = \frac{1.1 r_c q''}{k_l \sin\theta_r} + \frac{2\sigma \sin\theta_r\, T_{sat}}{r_c \rho_v h_{lv}} \quad (4)$$

1.4 Need for enhancement:

Boiling can serve as a potential cooling method for high powered electronic systems, compact heat exchangers and core of nuclear reactors. This advantage can be tapped to develop heat transfer surfaces by passive enhancement techniques. It is essential to develop a surface that can dissipate large amount of heat at considerably low wall superheats. A surface with high heat transfer coefficient can be utilized to cool the above mentioned devices. Also, by delaying CHF a wider operating range can be achieved which improves the effectiveness of the surface. The target for this research is to achieve high heat dissipation rates in excess of 300 W/cm^2 and wall superheat less than 10 °C.

Figure 4 shows a pictorial representation of boiling enhancement. Two key objectives are to (i) reduce wall superheat and, (ii) increase CHF to prove the effectiveness of the tested surfaces.

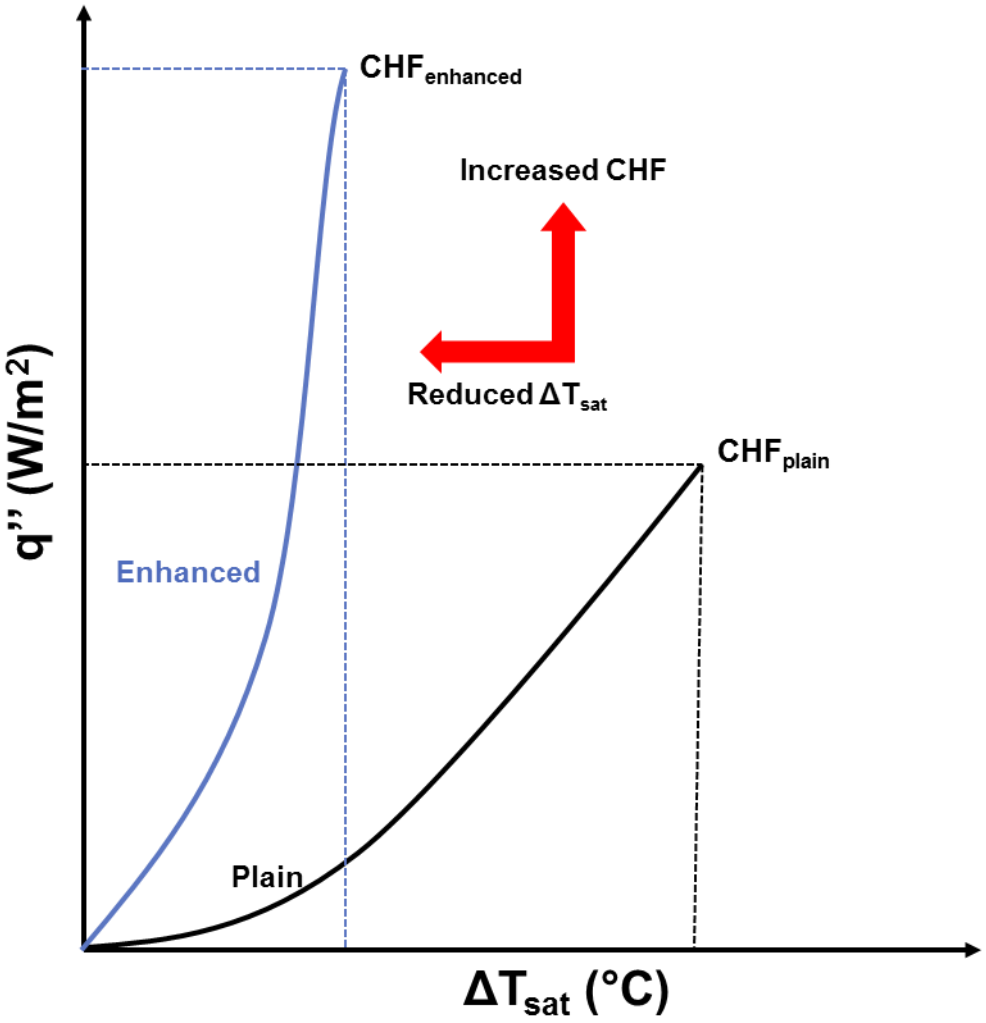

Figure 4. Pictorial representation of boiling enhancement

Chapter 2

In this chapter a detailed literature survey of different surface enhancements techniques is presented and the key understanding from the literature review is enumerated in the scope of this work.

2.1 Literature review

Researchers have resorted to different enhancement techniques to improve pool boiling performance. This chapter classifies the enhancement techniques based on porous, liquid wettability on heater surface, non-conventional techniques, artificial nucleation sites, fluids and micromachined surfaces and highlights the scope of the present work.

2.1.1 Enhancement techniques and previous work

The pioneering work conducted by Nukiyama [6] led to the understanding of boiling heat transfer. With a power controlled nichrome wire, he was able to develop a dependence of heat flux on the wall superheat to characterize boiling. Free convection, nucleate, transition and film boiling were identified as the different regimes in boiling. The performance of a heated surface is dependent on its morphology as shown by Bui and Dhir [7]. They used a clean mirror finish and an emery 600 sanded copper surface. The pool boiling performance indicates that rough surface was able to dissipate higher heat flux compared to a polished surface at the same wall temperature. Marto and Rohsenow [8] included a surface-fluid interaction factor C_{sf} in their widely accepted boiling correlation to relate heat flux to the wall superheat in the nucleate boiling region.

Nucleation in boiling is the process in which finite clusters of gas molecules appear in the bulk liquid as a second phase. Heterogeneous bubbles are those formed in the

crevices and cracks on the heater surface as against homogenous bubbles which are formed naturally and not from pre-existing vapor in grooves (crevices or cracks) on the surface. Hsu and Graham [2] and Hsu [3] developed a criterion for range of active nucleation sites as a function of subcooling, pressure and length of thermal boundary layer.

Fundamental mechanisms have shown that enhanced surfaces like open microchannels [9–11], microporous surfaces [12–14] ,nanostructures[15–17] and nanofluids [18–20] have significantly improved the heat transfer performance by increasing the heat transfer area or by affecting the liquid wettability on the surface.

2.1.3 Heat transfer enhancement – porous media

Porous surfaces have offered very high flux at relatively low temperature differences due to their increased surface area and availability of additional nucleation sites. Patil and Kandlikar [21] reviewed the different manufacturing techniques used to create porous surface for boiling heat transfer. The manufacturing techniques were classified into sintering, electrodeposition, and advanced techniques. Their study suggested sintering to be an easy and efficient technique to obtain porous structure with electrodeposition being a viable alternative using hydrogen bubble evolution. They also listed soldering, brazing, binding with alloys, chemical vapor deposition etc. under advanced techniques. In their subsequent publication [22,23], a heat transfer surface was developed with porous microchannel fin tops using two step electrodeposition, and reported a CHF of 325 W/cm^2 at a wall superheat of 7.3 °C. Their high speed images reveal that bubbles nucleated on the fin tops which facilitated liquid re-entry into the channels aiding convection similar to a jet impingement.

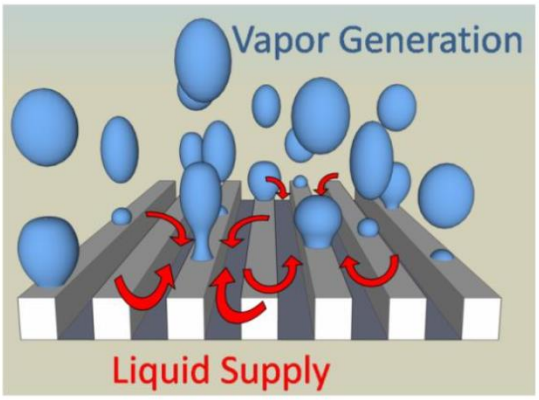

Figure 5. Vapor generation mechanism proposed by Patil and Kandlikar [23]

Nukayama et al. [26] suggested three fundamental evaporation modes (flooded mode, suction evaporation mode and dried up mode) responsible for boiling heat transfer in porous surfaces. Suction evaporation mode is identified as an effective region to dissipate large heat flux. Li and Peterson [27] conducted a study on porosity, pore size and thickness of sintered copper mesh structure. Their study on three pore sizes, 119.2 μm, 140 μm and 232.2 μm, suggested that smaller pore size was better for heat transfer performance. In terms of CHF, a thicker coating increased the CHF whereas a thin coating contributed to low wall superheats.

Webb [28] conducted a series of boiling experiments to study different geometric variables like particle diameter, coating thickness and pore size of copper porous coatings. The results indicate that a maximum boiling coefficient is obtained with a coating thickness of roughly three to four times particle diameters for highly conductive surface like copper but this finding does not hold true for low thermal conductivity materials like bronze. Furthermore he suggested that pore size has a significant effect than particle size. The paper also identifies the requirement to understand vapor-liquid phenomena in the pores. Afgan et al. [29] conducted pool boiling tests with distilled

water, R-113 and ethanol on horizontal tubes to understand the effect of hysteresis. The tube was coated with sintered metal layers of spherical or dendritic particles. Boiling hysteresis was observed for coating thickness of over 1mm with water. It was concluded that for highly wetting liquids, hysteresis was observed for all coating thickness.

Bergles and Chyu [30] conducted boiling tests on porous metallic coatings to understand the effect of hysteresis. The degradation characteristics of porous surfaces are studied for commercial application of these surfaces with water and R-113. They observed that nucleation takes place within the porous matrix and these reentrant cavities are not subjected to flooding. Mudawar and Anderson [12] studied different enhancement techniques like fins, studs, grooves and vapor trapping cavities by having the heater surface in vertical orientation with FC-72 and FC-87. Heat fluxes in surplus of 100 W/cm^2 with saturated FC-72 were reported for cylindrical enhanced surfaces. They also concluded that artificial cavities larger than 0.3 mm were ineffective in lowering wall temperature.

Some non-conventional techniques have been used by researchers to increase CHF. Mori and Okayuma [31] created a heat transfer surface by attaching a honeycomb structure to the heated surface and investigated the effect of height of the structure on the pool boiling performance. They reported a CHF of 250 W/cm^2 which was approximately 2.5 times higher than a plain surface. They identified capillary action and reduction of flow resistance due to separate vapor and liquid flow paths as the contributing factors to CHF enhancement.

2.1.4 Heat transfer enhancement – liquid wettability and artificial nucleation sites

Nanoscale coatings by electrodeposition process have contributed to improved liquid wettability which has enhanced boiling heat transfer. Yao et al. [16] grew copper nanowires with 200 nm diameter and 5-10 μm height on flat copper substrate using anodized aluminum oxide templates and electrodeposition process. A boiling performance of 164 W/cm^2 at a wall superheat of 11 °C was reported owing the improvement to increased heat transfer area and coupling effects of micro/nanoscale cavities which affected the bubble dynamics associated with pool boiling. Ahn et al. [32] deposited nano sized zircaloy-4 on a surface to decrease the contact angle of water which increased liquid wettability contributing to enhanced performance.

Artificial nucleation sites are fabricated on test surfaces to force bubble nucleation at select locations on heated surface. Sato et al. [33] drilled cylindrical holes 10 μm in diameter and 40 μm deep on a mirror finished silicon wafer by applying photo resist and subjecting to ultraviolet rays. It was observed that with narrow cavity spacing, the convection created by departure of the bubble was the main source of heat transfer at low heat fluxes. As the heat flux increased, latent heat was proposed as the contributing factor for heat transfer. At a wider cavity spacing, larger bubble diameter influenced convection to be the dominant heat transfer contributor.

2.1.5 Heat transfer enhancement - fluids

Fluid enhancement is an alternative technique to increase CHF. Concurrent to water, different fluids like, Fluorient liquids, are investigated to establish the performance of enhanced surfaces[34–36]. Ethanol is an alternative to refrigerants due to its higher heat

transfer performance and higher heat of vaporization. Kalani and Kandlikar [11] tested microchannel copper chips with ethanol as the working fluid and established that deeper channel depth (400 μm), narrow channel width (200 μm) and narrow fin width (200 μm) had the best performance dissipating 120 W/cm^2 at a wall superheat of 17 °C. Hegde et al. [37] investigated the effect of CHF using CuO nanofluids at various concentrations. They reported a CHF enhancement of 130% for a volume concentration of 0.2%. The deposition of nanoparticles on the heater surface forming a coating was identified as the contributing factor to CHF enhancement.

2.1.6 Heat transfer enhancement - micromachined

Researchers have explored rectangular fins or micro fins used with various fluids; all of which have resulted in increased heat transfer performance due to area enhancement. Pastuszko and Piasecka [38] experimentally studied the effect of pool boiling performance on mini fin arrays and micro cavities with water and FC – 72 at atmospheric pressure. Mini fins of 0.5 mm and 1 mm and micro cavities of depth 15 – 30 μm were fabricated by spark erosion technique. Their study suggested that micro cavities provided additional nucleation sites which contributed to intensification of heat flux. Furthermore, they suggested mini fins with 1 mm height provided effective boiling heat transfer intensification for water at heat fluxes higher than 70 W/cm2. Pastuszko [39] studied the effect of fin height, pore diameters and tunnel pitch of tunnel surfaces fabricated from a 0.05 and 0.1 mm thick perforated copper foil with pore diameters of 0.3, 0.4, 0.5 mm sintered with mini fins of height 5 and 10 mm. A heat transfer coefficient of 50 kW/ m^2-$^{\circ}$C is reported for water which was 3 – 4 times higher than smooth fins.

Rainey et al. [40] experimentally studied the effects of pressure, subcooling and non-condensable gas of microporous enhanced square copper pin fin array with FC – 72 as the working fluid on nucleate boiling and CHF. Their study revealed that for saturated liquid with microporous finned surfaces, CHF value decreased linearly with increasing fin length. They attributed this effect to decreased fin tip temperatures. Furthermore, their research suggested that horizontal orientation of heater surfaces performed better than its vertical counterpart. Guglielmini et al. [41] conducted a series of studies for different geometries on square pin fin array with FC-72 as the working liquid. They concluded that longer fins performed better when the fins are uniformly spaced and also finned surfaces significantly increases heat transfer coefficient at low heat fluxes.

Kandlikar [42] implemented contoured fin as a surface enhancement technique based on separate liquid and vapor pathways using evaporation momentum force. A CHF of 300 W/cm^2 at a low wall superheat of 4.9 °C with a record heat transfer coefficient of 629,000 W/m^2-°C is reported. The paper further suggested that evaporative momentum force becomes dominant at high heat flux which significantly staves off CHF. Cooke and Kandlikar [10] conducted pool boiling tests on open microchannel copper chips fabricated by micromachining and reported a heat flux of 244 W/cm^2 which was 5 times larger than that of a plain chip at the same wall superheat. Their findings suggested that wider channels (> 350 μm), thinner fins (< 200 μm) and deeper fins (> 400 μm) were the best performing chips. Larger bubbles played a more significant role in rewetting the surface by inducing larger volume of liquid entry.

A summary of the best performing surfaces is tabulated in table 1.

Table 1. Summary of best performing surfaces in literature

Author's	Surface modification	Liquid	q'' (W/cm^2)	ΔT (°C)	h ($kW/m^2°C$)
Cooke and Kandlikar	Open microchannel	Water	244	9.8	269
Kandlikar	Contoured fin	Water	300	4.9	629
Li and Peterson	Sintered mesh	Water	367	63.7	57
Patil and Kandlikar	Open microchannel with porous fin tops	Water	325	7.3	445
Mori and Okayuma	Honey comb structure	Water	250	49.3	50
Chang and You	Low fin	FC-87	22	23	-
Chang and You	ABM coated	FC-87	13	14	-
Mudawar and Anderson	Tall fins	FC-87	20	29	-

2.2 Scope of work

As seen from literature, surface and fluid enhancement has resulted in significant improvement in the heat transfer rate with improved performance, enhanced CHF and reduced wall superheats. This research focuses on pool boiling performance of open microchannels with cross-linked flow as an enhanced heat transfer surface with water as the working fluid at atmospheric pressure. The hypothesis aims at coupling area enhancement technique and better microconvective liquid irrigation pathway to the heated surface to amplify the performance.

Liquid re-circulation in microchannels is a critical factor to enhance performance and delay CHF. The underlying mechanism proposed by Cooke and Kandlikar [10] is developed further to facilitate liquid re-entry into the channels to stave off CHF. At CHF,

a vapor blanket covers the microchannel which inhibits liquid supply to the nucleation sites. In order to facilitate this liquid supply, disjunctions in the fins are proposed to serve as liquid pathways as shown in Fig. 6. These disjunctions added to an open microchannel can be considered as cross-linked channels. It is postulated that the liquid will flow from the bulk region down into the microchannels through these gaps. Also, these cross-linked channels are proposed to provide additional nucleation sites which will enhance the performance further.

The geometry of the channel is chosen based on the conclusions drawn by Patil and Kandlikar [23]. They concluded that the best performing chip was with a channel width=500 μm, fin width=200 μm and fin depth=400 μm and hence to amplify the performance the same microchannel dimensions are used in this study.

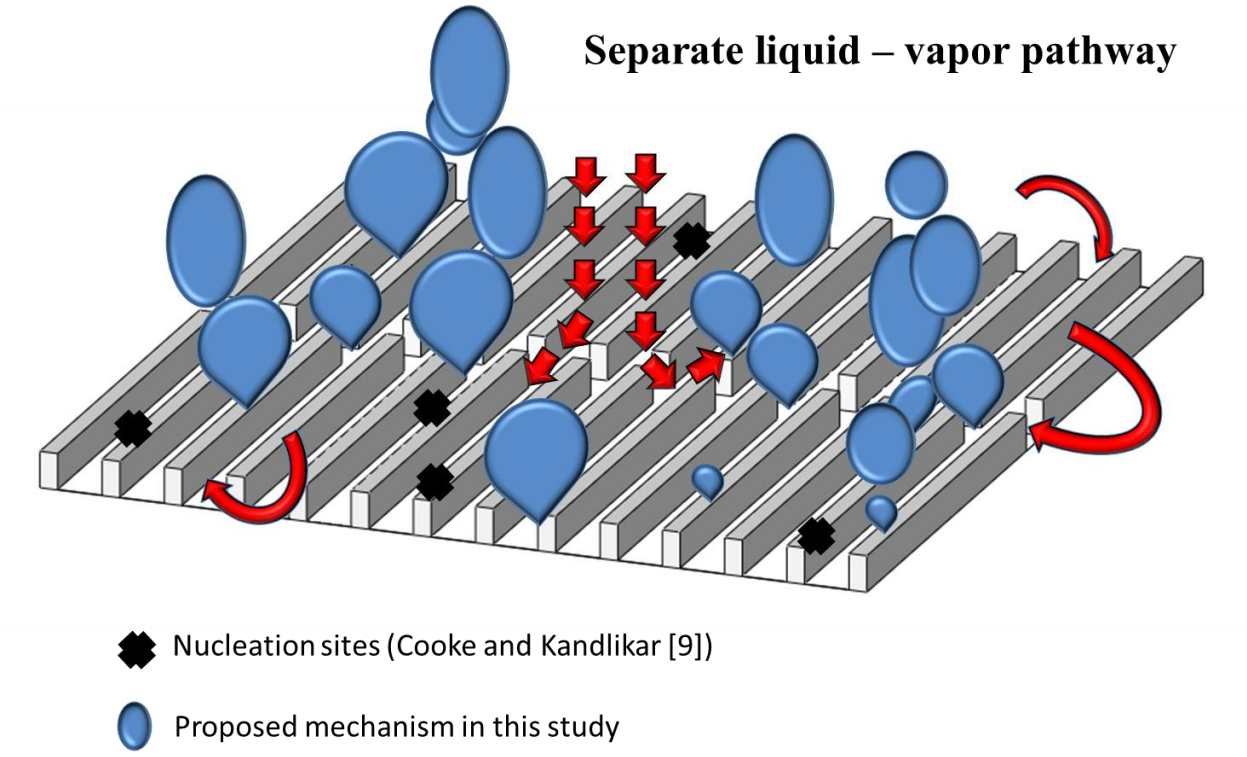

Figure 6. Proposed liquid-vapor pathway

Chapter 3

Pool boiling experimentation procedure, results and visualization images with water are discussed here.

3.1 Experimental setup

Fig. 7 shows the schematic of the pool boiling test setup. The bottom garoloite plate consisted of a ceramic chip holder to hold the heater surface over which a quartz glass water bath measuring 14mm × 14 mm × 38 mm is assembled by means of 4 stainless steel socket head cap screws (1/4'' diameter). A glass water bath is used chiefly to aid visualization and is sealed to the ceramic chip holder by means of a rubber gasket which covers the area outside the boiling surface. A middle plastic plate holds the water bath on the upper side and is connected to the top aluminum plate by means of 2 stainless steel socket head cap screws (1/4'' diameter). A water reservoir is mounted between the middle plastic plate and top aluminum plate. The water reservoir is sealed with rubber gaskets on either side to ensure against leakage at all times. The top aluminum plate is provided with two circular openings for the saturation thermocouple probe and a 60-VDC, 200 W auxiliary cartridge heater to maintain water in the reservoir at saturation by boiling continuously.

The bottom section of the setup consists of a 120-VDC, 4 × 200 W capacity cartridge heater inserted into a copper heater block similar to Kalani and Kandlikar [43]. The copper block consisted of a truncated portion measuring 10 mm × 10 mm × 40 mm that fits into the groove on the bottom side of the ceramic chip holder. This ensured that 10 mm × 10 mm surface of the heater is in contact with the test chip which also has a base

section measuring 10 mm × 10 mm which facilitated 1D conduction from the heater to the test chip. Additionally, the copper block is housed on a ceramic sleeve to minimize heat losses. Four compression springs supported the bottom aluminum plate that provided the required degree of movement to establish contact between the test chip and the heater and accommodate for any expansion during the testing. A shaft pin (3/8'' diameter) connected the middle garolite plate, bottom garolite plate and the work desk which ensured stability of the setup.

A National Instruments cDaq-9172 data acquisition system with NI-9213 temperature module was used to record the temperature. A LabVIEWVR virtual instrument displayed and calculated the surface temperature and heat flux.

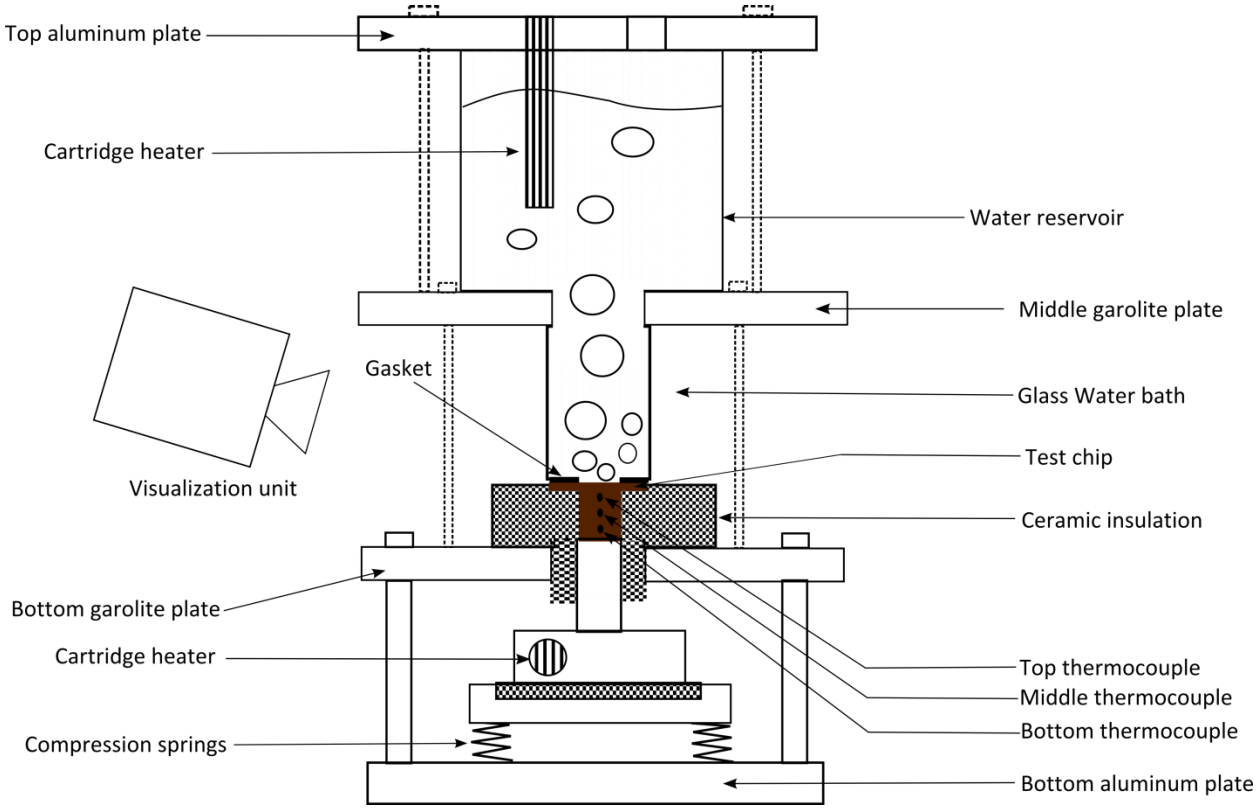

Figure 7. Schematic of experimental setup used for testing with water

3.2 Test chips

The test chips used in this study were 17 mm × 17 mm × 9 mm as shown in Fig. 8. The heater side consisted of a 10 mm × 10 mm × 9 mm protrusion with three 0.762 mm holes drilled 3 mm apart to accommodate the thermocouples as shown in Fig. 9. The effect of contact resistance in the heat flux calculation is eliminated by placing thermocouples in holes drilled in the test chip. Three K-type thermocouples are inserted into these holes to read the temperature at different locations on the chip.

As stated previously, microchannel dimensions are chosen based on best performing chip reported in literature. The location of the cross-linked channels (channel width = 500 μm) are as shown in Fig 7. On the 10 mm × 10 mm boiling surface, equal fin bank widths of 4.75 mm, 3mm, 2.125 mm and 1.6 mm are machined for 1, 2, 3 and 4 cross-linked microchannels respectively.

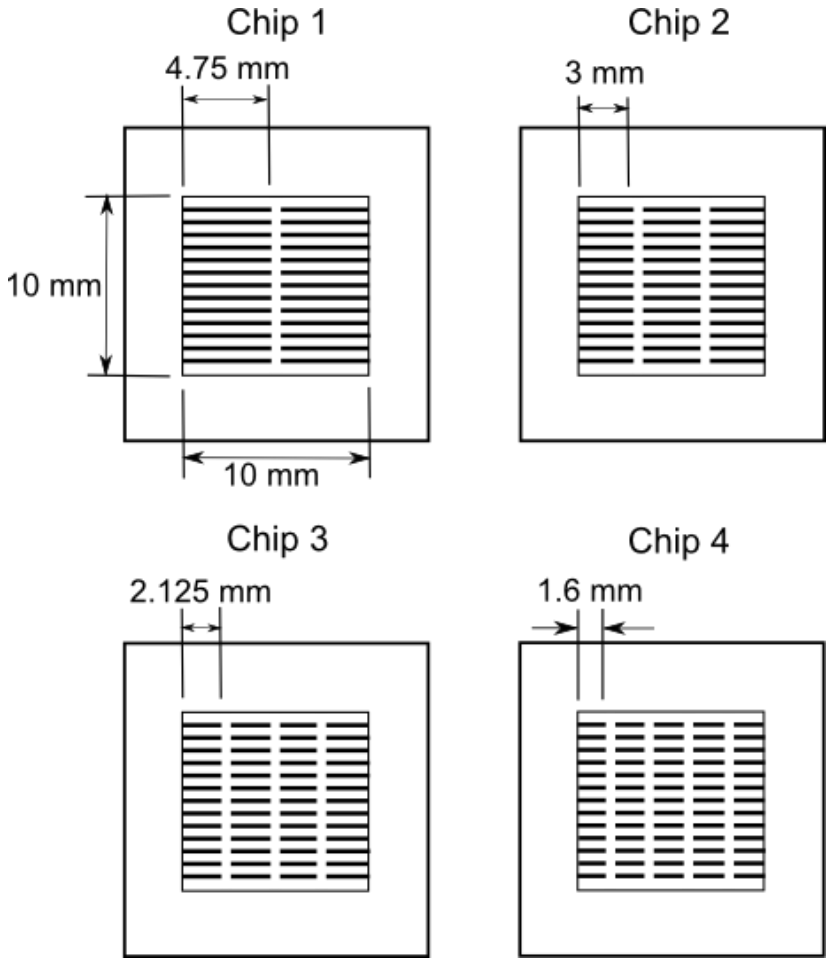

Figure 8. Cross-linked open microchannels investigated in this study

The heat flux to the test section was calculated using 1D conduction equation

$$q'' = -k_{Cu}\frac{dT}{dx} \tag{4}$$

where, the temperature gradient dT/dx was calculated using the three point backward Taylor's series approximation

$$\frac{dT}{dx} = \frac{3T_1 - 4T_2 + T_3}{2\Delta x} \tag{5}$$

where, T_1, T_2, T_3 are the temperatures corresponding to the top, middle and bottom of the test chip under study.

The boiling surface temperature was obtained by using eq. (4) and is given by,

$$T_{wall} = T_3 - q'' \left(\frac{x_1}{k_{Cu}}\right) \quad (6)$$

where, T_{wall} is the boiling surface temperature and x_1 is the distance between the boiling surface and thermocouple T_3 which is equal to 1.5 mm.

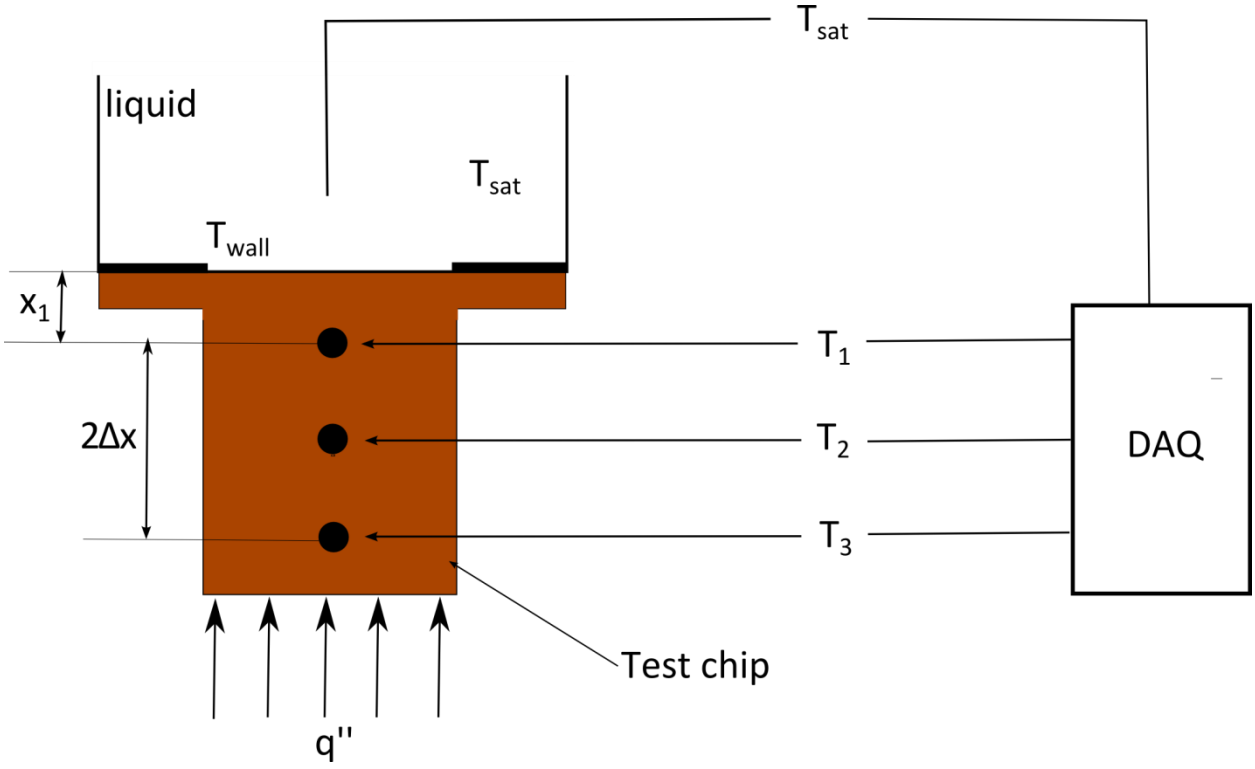

Figure 9. Schematic of heater assembly and data acquisition

Cooke and Kandlikar [10] have shown that open microchannel geometry with water as the working medium yielded high performance. In this study, open microchannels with cross linked flow have been identified as the heat transfer surface. This type of surface enhancement has not been investigated in pool boiling with water as the working liquid. The cross linked microchannels were fabricated using CNC machining on a 10 mm × 10 mm area on the boiling surface of the chip. The test matrix shown in table 1 exhibits the

microchannel dimensions used in the study. The dimensions are reconfirmed by measuring using a laser confocal microscope and scanning electron microscope image. The pool boiling performance on the number of cross channels is the parameter investigated in this study.

3.3 Uncertainty analysis

Two main errors that arise during experimentation are bias errors and precision errors. The bias errors are due to errors from calibration and precision errors are due to sensitivity of the testing devices. A thorough uncertainty analysis was performed, similar to Patil and Kandlikar [23] and Cooke and Kandlikar [10].

Cumulatively, the errors due to bias and precision can be expressed as,

$$U_y = \sqrt{B_y^2 + P_y^2} \tag{7}$$

Where, U_y is the uncertainty or error, B_y is the bias error and P_y is the precision error. The parameters contributing to errors are thermocouple calibrations, thermal conductivity of copper and the distance between the thermocouple spacing on the test chip. The thermocouples are calibrated and its precision error was computed statistically to be ± 0.1 °C with due consideration of calibration accuracy and precision.

Each individual error that propagated due to measurement in temperature (both heater and surface temperature) and also distance between thermocouple spacing are calculated using the equation below,

$$U_p = \sqrt{\sum_{i=1}^{n} \left(\frac{\partial p}{\partial a} * u_{ai}\right)^2} \quad (8)$$

Where U_p is the uncertainty in the parameter p, and u_{ai} is the uncertainty of measured parameter a_i. The uncertainty in the heat flux can thus be expressed by the following equation.

$$\frac{U_{q"}}{q"} = \sqrt{\left[\left(\frac{U_k}{k}\right)^2 + \left(\frac{3U_{T_1} * k_{Cu}}{\Delta x * q"}\right)^2 + \left(\frac{4U_{T_2} * k_{Cu}}{\Delta x * q"}\right)^2 + \left(\frac{U_{T_3} * k_{Cu}}{\Delta x * q"}\right)^2 + \left(\frac{U_{\Delta x}}{\Delta x}\right)^2\right]} \quad (9)$$

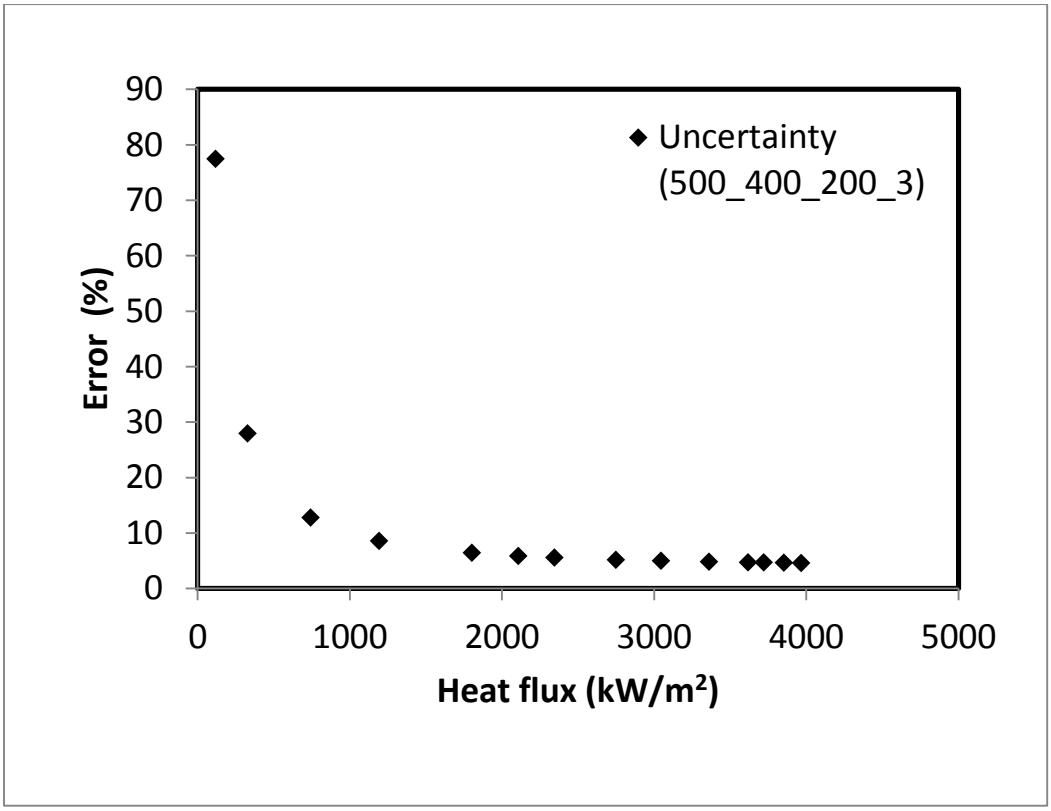

Figure 10. Plot showing variation of uncertainty with heat flux

Based on the uncertainty values a graph of error in heat flux is plotted against the corresponding heat flux values. It is evident from the plot that at low heat flux an error of

77 % is observed whereas at higher heat flux which defines the range of interest the error plateaus at less than 5 % as shown in Fig. 9.

To ensure 1D conduction a heat loss study is performed as shown in Fig. 10. Based on Fouriers's law of conduction, the temperature profile across the test section is expected to be linear. Fig.6 shows a plot of temperature distribution for 39 W/cm^2, 100 W/cm2 and 171 W/cm^2 which depicts linear progression with R squared value close to 1 which ensured minimal heat loss during the experimental process.

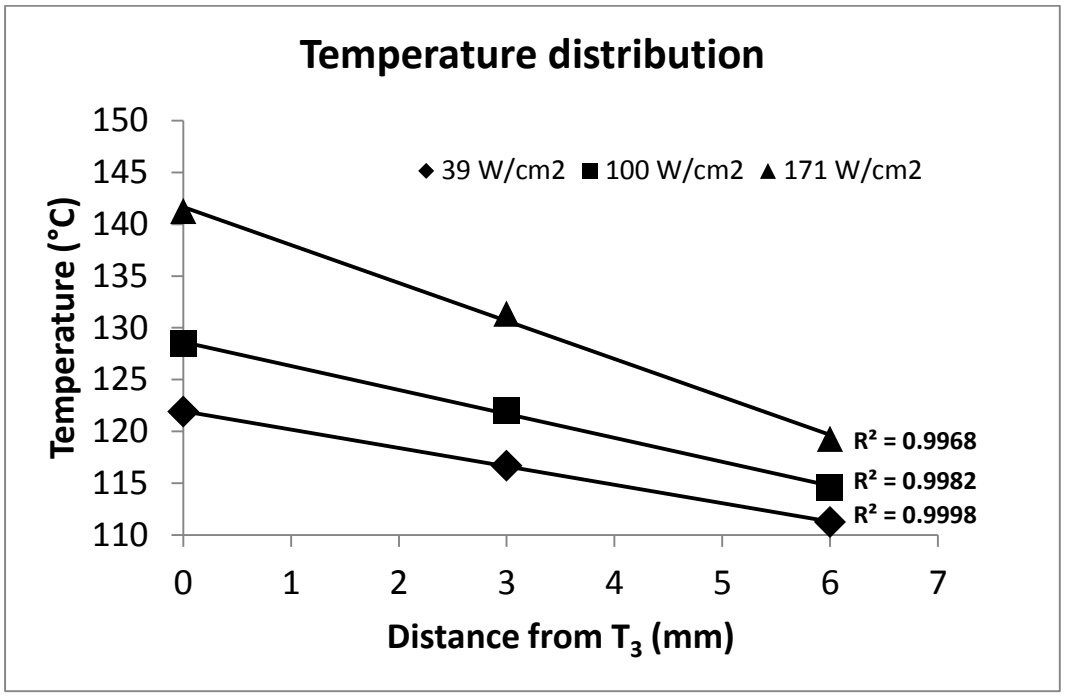

Figure 11. Heat loss study showing variation of temperature over the distance

3.4 Results

Pool boiling experiments were conducted with distilled water at atmospheric pressure over cross linked microchannel to obtain a trend on the effect of number of cross channels. As a baseline comparison, distilled water was boiled over a plain surface. The test matrix is as shown in Table 3 and consisted of 4 chips with the same microchannel

dimensions as shown in Table 2. Each chip is named in the order of channel width, channel depth, fin width and number of cross linked channels. For example, if there is 1 cross linked channel it is named as 500_400_200_1. The only variable parameter in the experimentation was the number of cross linked channels.

Table 2: Cross linked microchannel dimension

Microchannel parameter	Fin width	Channel width	Channel depth	Cross linked channel
Value (μm)	200	500	400	500

The results were presented in terms of a pool boiling curve which depicted the heat flux dissipated at certain wall superheat. The heat flux is computed individually using both the projected area and normalized surface area of the test chips. The wall superheat is defined as the difference in temperature between the surface of the chip and saturation temperature of the fluid (distilled water).The surface temperature is calculated as the temperature at the top of each microchannel chip. Also, a heat transfer performance curve which is a plot of heat transfer coefficient versus heat flux revealed the performance of the chip compared to a plain chip.

3.4.1 Comparison between plain chip and cross linked channels:

Firstly, distilled water is allowed to boil on a plain chip to serve as the baseline for all enhancement comparisons. The plain chip surface is obtained by rubbing on sand paper with a fine grit size of 200. Cross linked microchannel with 1 cross channel (Chip 1) is boiled to draw an estimate on the degree of enhancement. The cross linked microchannel showed significant enhancement with a CHF of 352 W/cm^2 at a wall superheat of 14 °C as against a plain chip which had a CHF of 125 W/cm^2 at a wall superheat of 40 °C which

corresponds to an enhancement of 180% in CHF over a plain chip as shown in Fig. 11. It is evident from the Fig. 11 that cross linked microchannel had a steeper slope when compared to a plain chip. This proved that cross linked microchannel shifted the pool boiling curve to the left compared to a plain surface and provided wider operating range by delaying CHF.

3.4.2 Parametric study

Figure 11 shows a comparison of pool boiling curves for cross linked microchannels with 1 (chip 1), 2 (chip 2), 3 (chip 3) and 4 (chip 4) cross-linked channels. The main objective of this parametric study was to identify a trend in the pool boiling performance and validate a suitable mechanism from literature. All the test chips were pushed to CHF to determine the maximum performance of these surfaces. The CHF and wall superheat values are tabulated as shown in Table 2. The best performing chip with 3 cross linked channel dissipated 396 W/cm^2 at a low wall superheat of 7.4 °C which translates to an enhancement of 217% in CHF compared to a plain surface. The chips with 1, 2 and 4 cross channels had CHF value of 352 W/cm^2, 288 W/cm^2 and 255 W/cm^2 at wall superheats of 14.27 °C, 12.37 °C and 16.07 °C respectively. A detailed discussion of trends observed for CHF and HTC is presented in the discussion section. The worst performing chip with 4 cross linked channels had a CHF of 255 W/cm^2 which is comparable to the best performing chip reported by Cooke and Kandlikar [10] which is 244 W/cm^2. This goes to show that cross linked microchannel is an enhancement over a parallel open microchannel yielding high CHF values.

It can be seen that even number of cross linked channels had a CHF value less than 300 W/cm^2 whereas odd number of cross linked channels had CHF value in the range of

350 – 400 W/cm^2.The results are supplemented with high speed images which reveal bubble dynamics in the channels at low heat flux. The images suggested that a similar mechanism to [10] is observed and is explained in detail in the discussion section.

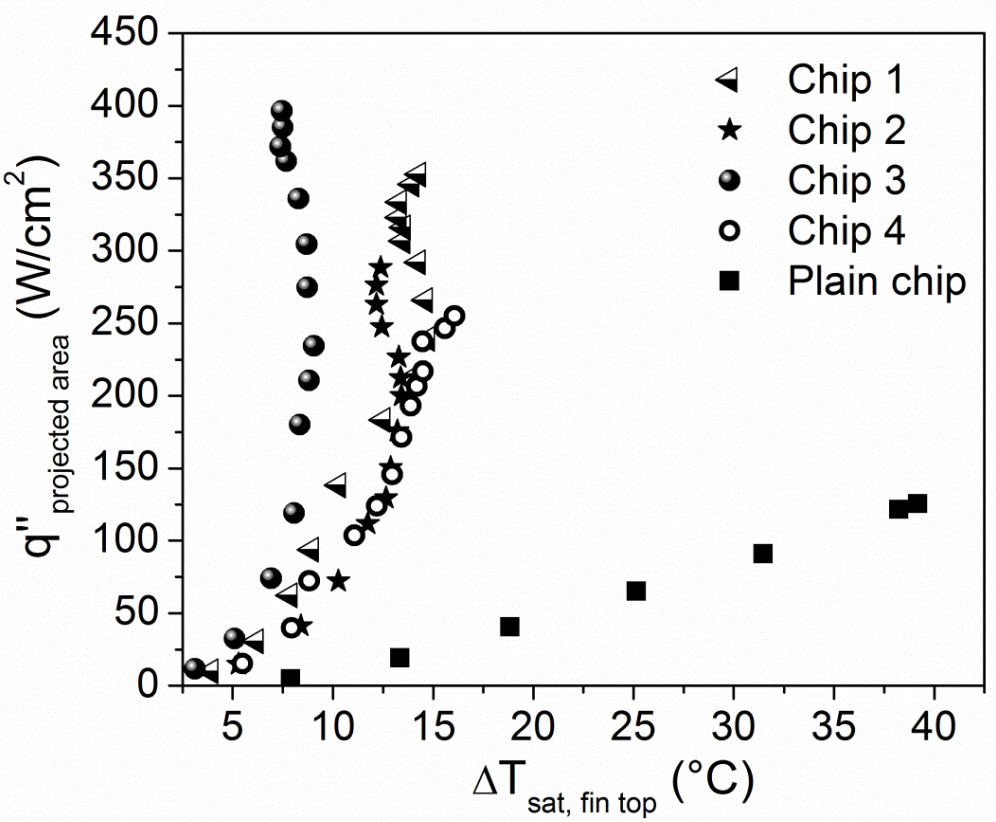

Figure 12: Boiling curves for plain and cross linked microchannel surfaces with water at atmospheric pressure with fin top temperature

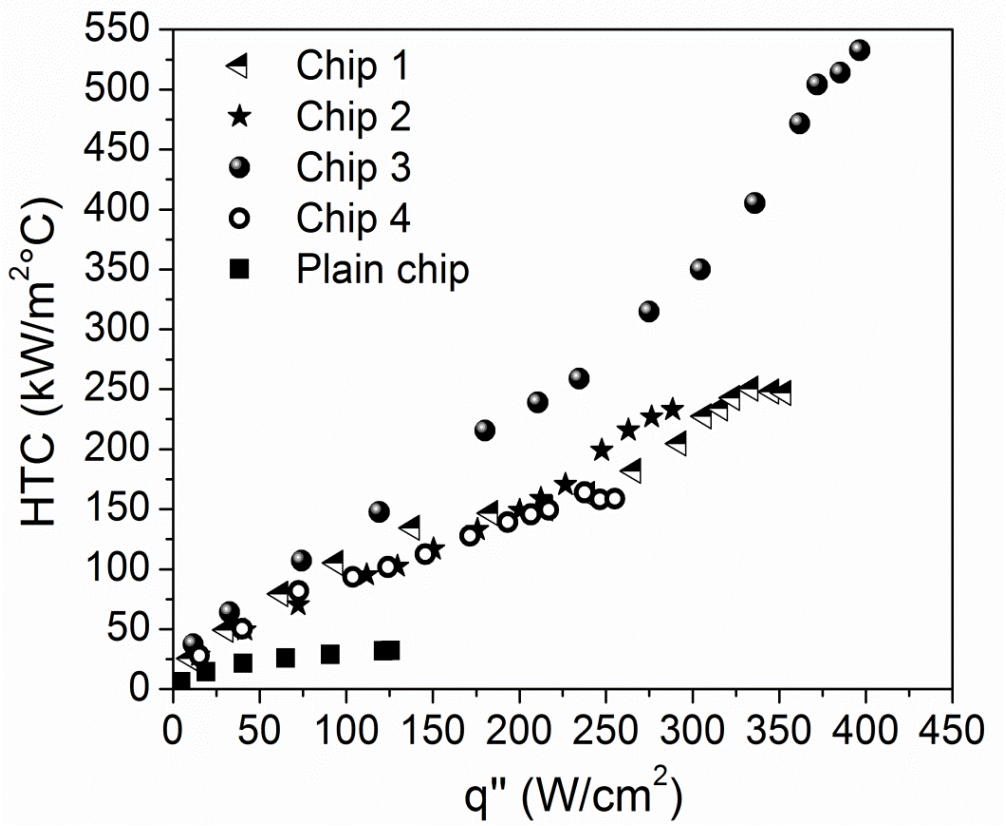

Figure 13: Heat transfer coefficient comparison for plain and cross linked microchannel surfaces using fin top temperature

Figure 12 shows the variation of HTC plotted against heat flux. No observable trend can be established but it is evident from the curves that cross linked channels with 1, 2 and 4 cross channels had similar heat transfer performance. At CHF, HTC of 246 kW/m^2-°C, 233 kW/m^2-°C and 158 kW/m^2-°C is observed for chips with 1, 2 and 4 cross linked channels respectively. Cross linked microchannel with 3 channels had the best performance with a HTC of 532 kW/m^2-°C representing an enhancement of 167% at CHF over a plain chip.

Table 3: Test matrix and results

Chip #	Chip dimensions(a_b_c)_crosslinks(d)	CHF (W/cm^2)	Wall superheat	Area enhancement

			(° C)	factor
1	500_400_200_1	352	14	2.0462
2	500_400_200_2	288	12	2.0124
3	500_400_200_3	396	7	1.9786
4	500_400_200_4	255	16	1.9448

3.4.3 Comparison with literature

Fig. 13 shows the comparison between the best performing surface reported in this study and performance plots available in literature for other enhancement techniques [10,23,27,31,42]. The CHF of the chip reported in this study is higher than all values presented in the comparison. For example, Patil and Kandlikar [23] reported a CHF value of 325 W/cm^2 at a wall superheat of 7 °C, which is similar to cross linked microchannel with the same wall superheat but with a higher CHF (396 W/cm^2). Cross linked 0microchannel offers higher CHF compared to Kandlikar [42], however, the wall superheat is considerably higher. A significant extent of enhancement can be drawn when compared to Cooke and Kandlikar [10] although larger channel dimensions are used, cross linked channel is an area enhancement on open microchannels investigated by [10] which has shown stark improvement in providing higher CHF at lower wall superheats. Furthermore, CHF reported by Mori and Okayuma [31] and Li and Peterson [27] are in the range of 250 W/cm^2 and 325 W/cm^2 respectively but at very high wall superheats, in excess of 50 °C, as against CHF value of the best performing chip reported in this study. The wall superheats for all surfaces investigated in this study are in the range of 7 °C to 16 °C.

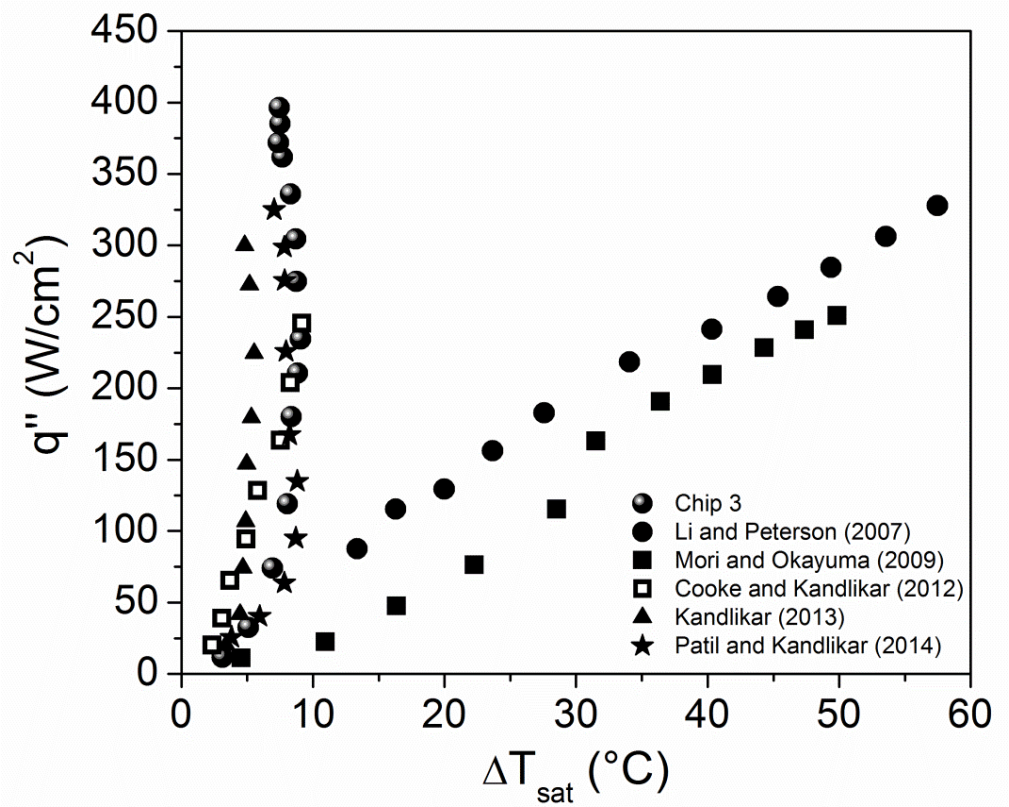

Figure 14: Comparison of best performing chip with other enhancements available in literature using fin top temperature [10, 23, 27, 31, 42]

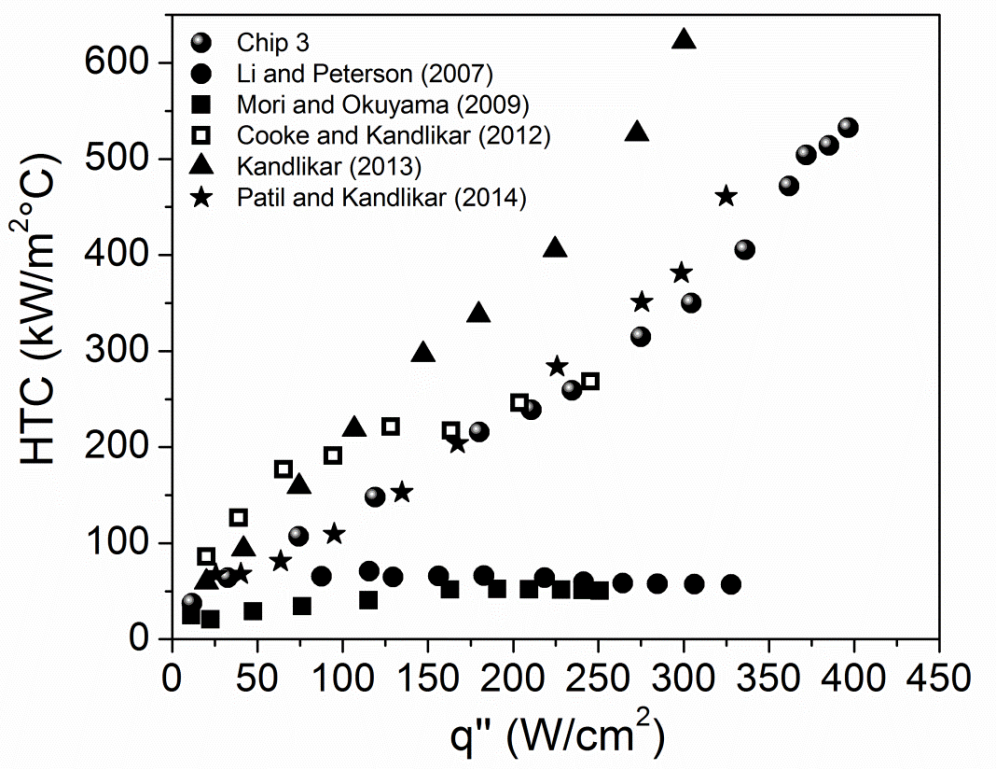

Figure 15: Comparison of heat transfer performance with other enhancement techniques available in literature

3.4.4 Hysteresis study:

A hysteresis study was performed to understand any losses that may occur during the cool down cycle. Fig. 15 shows the heating and cooling curves for test surfaces with 2, 3 and 4 cross channels. Firstly, 2 and 4 cross linked microchannels were pushed to a heat flux of around 230 W/cm^2 and subjected to reducing heat flux to observe any deviation in the two curves. Since cross linked microchannel with 3 cross channels had the best performance, it was pushed to 300 W/cm^2 and subjected to reducing heat flux. All the curves indicate minimal heat loss (hysteresis) ensuring repeatability at different surface temperatures within experimental errors discussed previously in the uncertainty analysis.

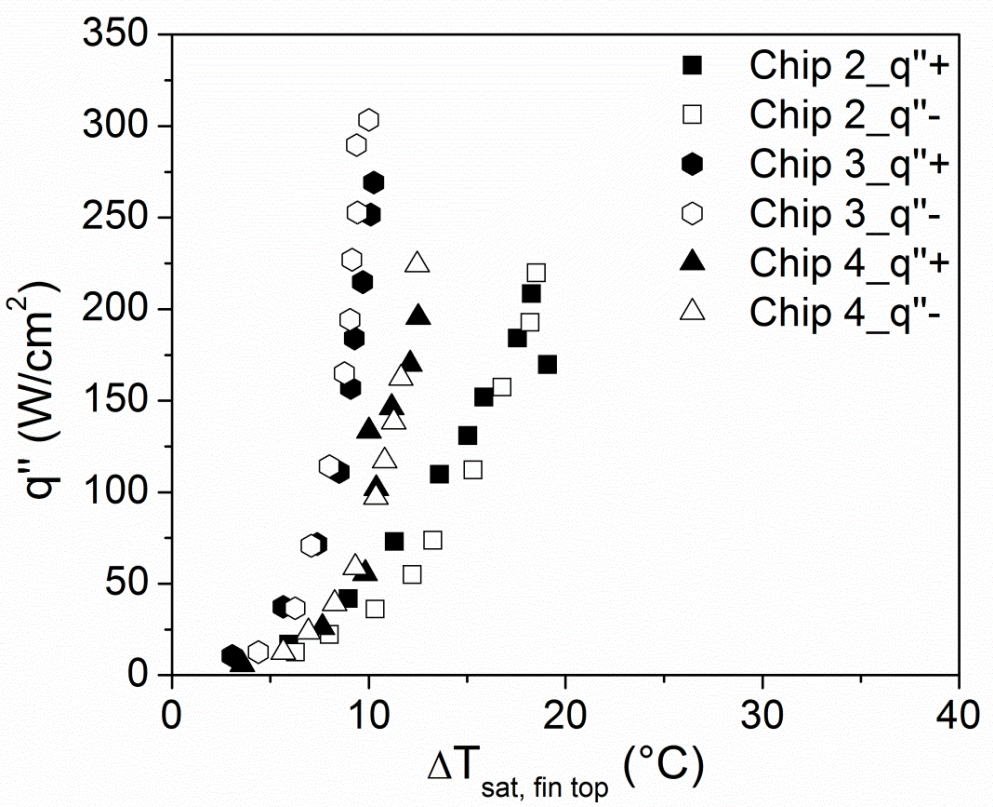

Figure 16: Heat transfer study to analyze hysteresis for 2, 3 and 4 cross linked channels

3.4.5 Normalized curves:

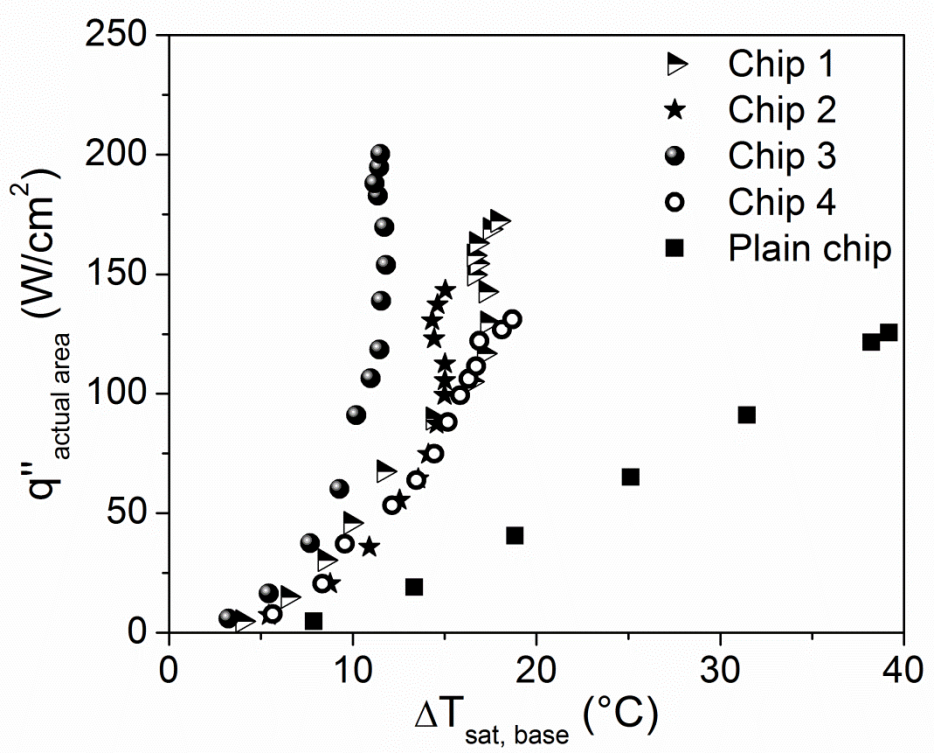

(a)

Figure 17: Normalized pool boiling curves to show area enhancement of cross linked microchannel surfaces using base temperature

Table 3 shows the surface area enhancement factor for different cross linked microchannels used in this study. The contributing factors to the area enhancements are number of channels, channel width and channel depth. The heat fluxes for the surfaces under investigation are divided by their respective area enhancement factors neglecting fin efficiency. The base temperature of the surface is considered in Fig. 17 which is a pool boiling curve of normalized heat flux plotted against the base temperature. Cross linked channel with 3 channels had a CHF of 200 W/cm^2 at a wall superheat of 11 °C which had an enhancement of 20% in CHF over a plain surface.

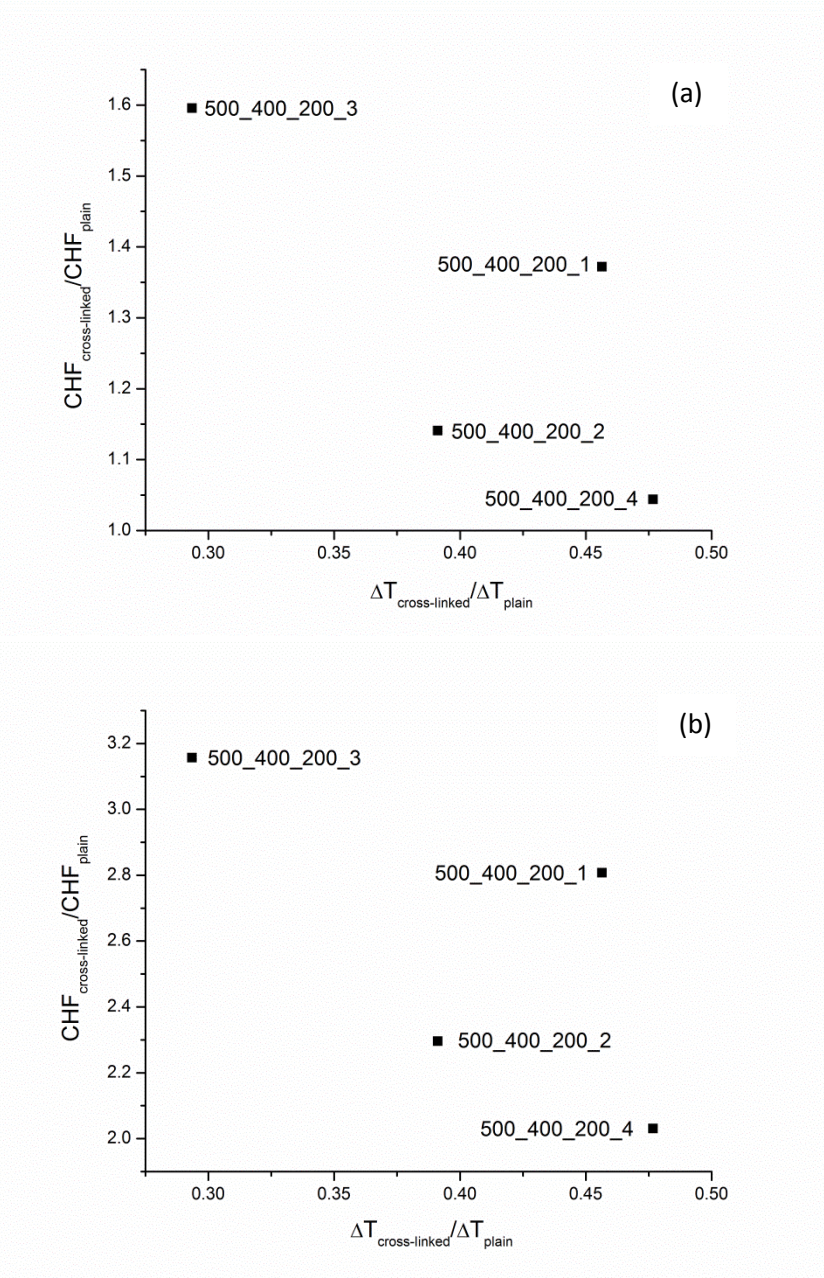

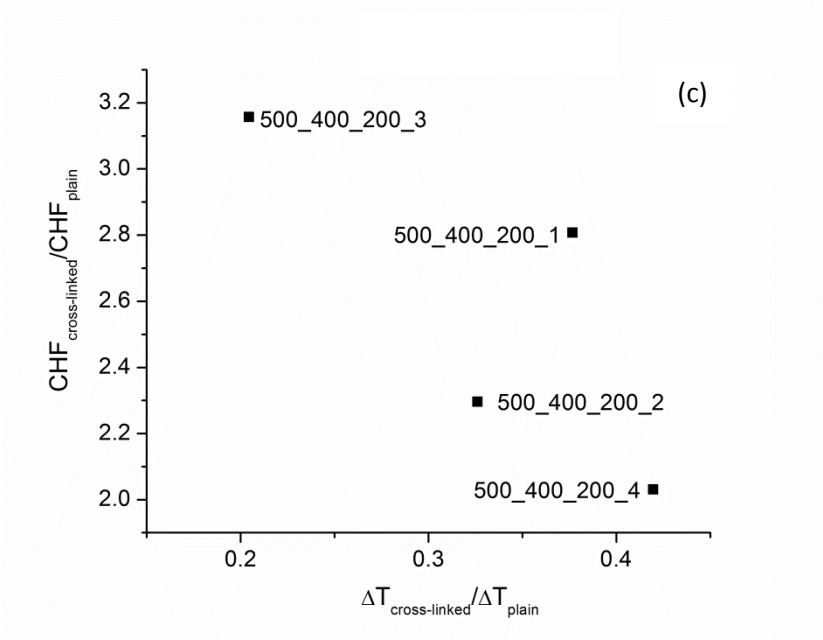

Figure 18. Plot showing the enhancement in CHF and wall superheat of cross-linked and plain chip considering (a) actual area and fin top temperature (b) projected area and fin top temperature (c) projected area and base temperature

Fig. 17 (a), (b) and (c) shows the degree of enhancement compared to a plain surface in CHF on the y-axis and degree of reduction in wall superheats on x-axis achieved for cross-linked microchannel with 1, 2, 3 and 4 cross-linked flow passages respectively. Fig. 13 (a) and (b) uses projected area to draw a trend on the degree of enhancement and Fig. 13 (c) uses actual area. When the projected area is considered, cross-linked microchannel with three cross-linked passages significantly contributes to delay in CHF and improved HTC as indicated by a threefold enhancement in CHF. A two fold enhancement in CHF is observed for 1, 2 and 4 cross-linked flow pathways. Furthermore, plots (a), (b) and (c) show a remarkable reduction in wall superheats as the values are less than one.

3.4.6 Discussion

The increased performance for all surfaces can be attributed to area enhancement and availability of additional nucleation sites. Furthermore, high speed imaging revealed

similar mechanism proposed by Cooke and Kandlikar [10]. Bubbles were formed at the corner regions on the bottom of channels and departed from the top of the fins which induced liquid inflow into the channels which was the chief contributor to low wall superheats and delayed CHF. Also, cross channels provided additional nucleation sites that contributed to increased heat dissipation.

Cross linked microchannels provided better irrigation pathways in the microchannels contributing to increased microconvective flow aiding liquid re-wetting in the channels which can also be identified as the main reason for the enhanced performance compared to microchannels without cross flow. At higher heat fluxes, availability of additional nucleation sites lead to increased liquid re-entry into the channels which contributed to delayed CHF.

3.4.6.1 Microchannel visualization images:

Two sets of images are shown in Figures 18 and 19. The images reveal similar bubble dynamics in the channels and at cross linked microchannel. At both locations, it can be clearly observed that bubbles nucleate at the bottom of the channel (Fig. 18, 19 (a)) and grow to the channel width (Fig.18, 19 (b)). In their departure route, they trace the sidewalls of the fin and eventually reach fin tops (Fig. 18, 19 (c)) and eventually depart from the two adjacent fin top surfaces (Fig. 18, 19 (d)).

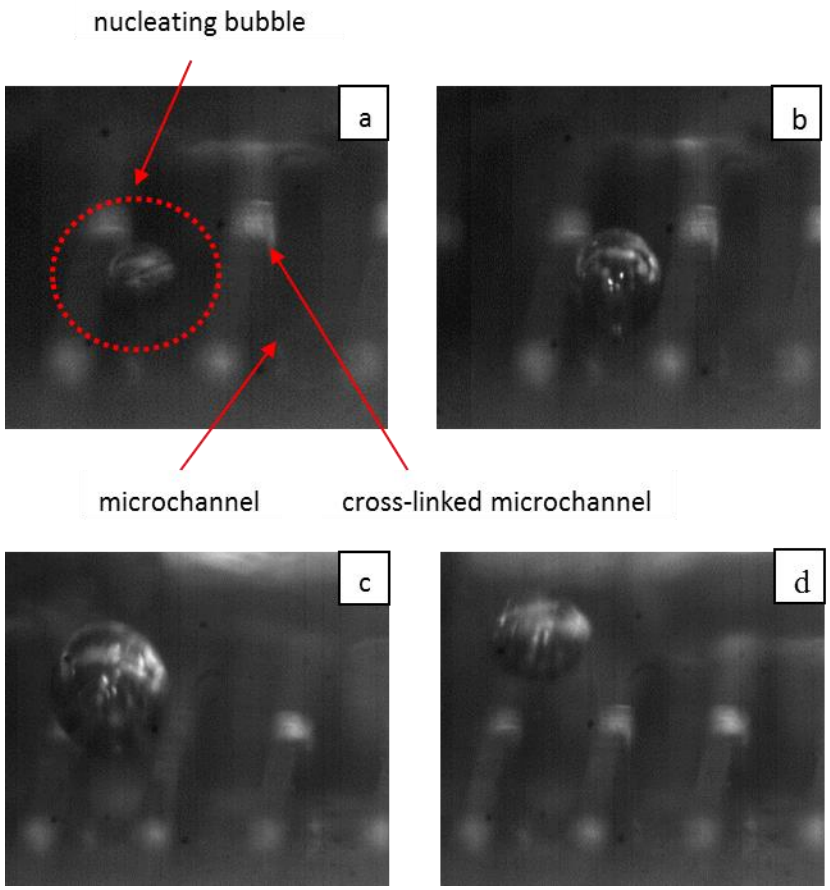

Figure 19 : Visualization set for microchannel displaying bubble dynamics at a heat flux of 13 W/cm^2 (a) bubble nucleation in channel bottom (b) Bubble growing to channel width (c) bubble rising to fin tops (d) bubble departing from fin top

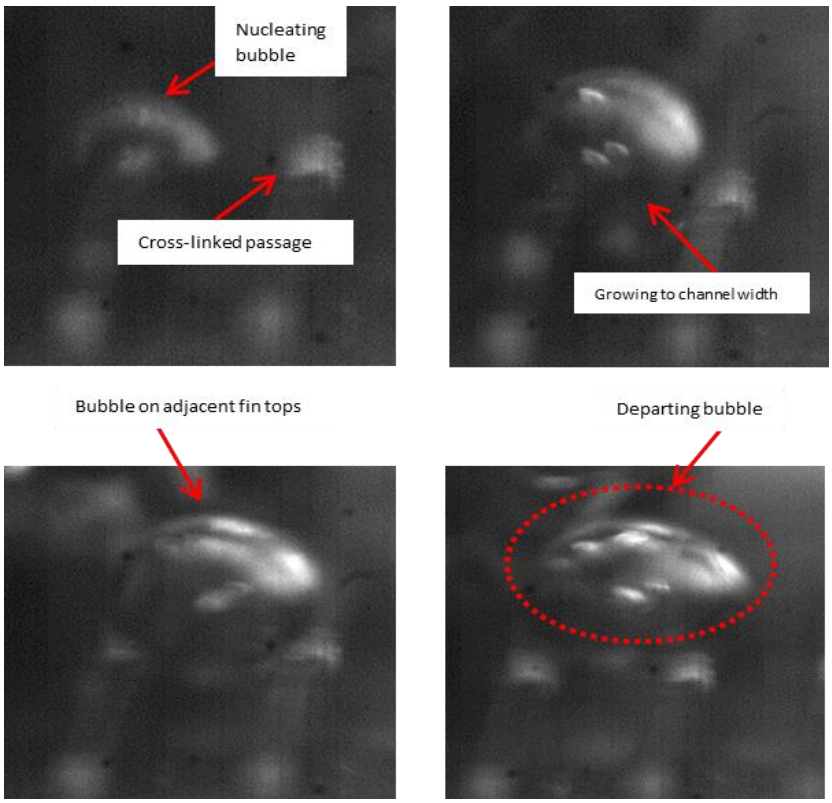

Figure 20. Visualization set for cross linked microchannel displaying bubble dynamics (a) bubble nucleation in channel bottom (b) Bubble growing to channel width (c) bubble rising to fin tops (d) bubble departing from fin top

3.4.7 CHF trend:

A definite trend in CHF is observed from the test surfaces investigated in this study. Fig. 20 shows a plot of CHF versus pitch of cross channels. As mentioned previously, it can be seen that odd number of cross linked channels yield higher CHF value as compared to even number of cross channels. It can be concluded from Fig. 19 that microchannel with 3 cross linked channel is the optimized surface to achieve high CHF at a considerably low wall superheat beyond which the performance drops significantly when 4 cross linked channels are used.

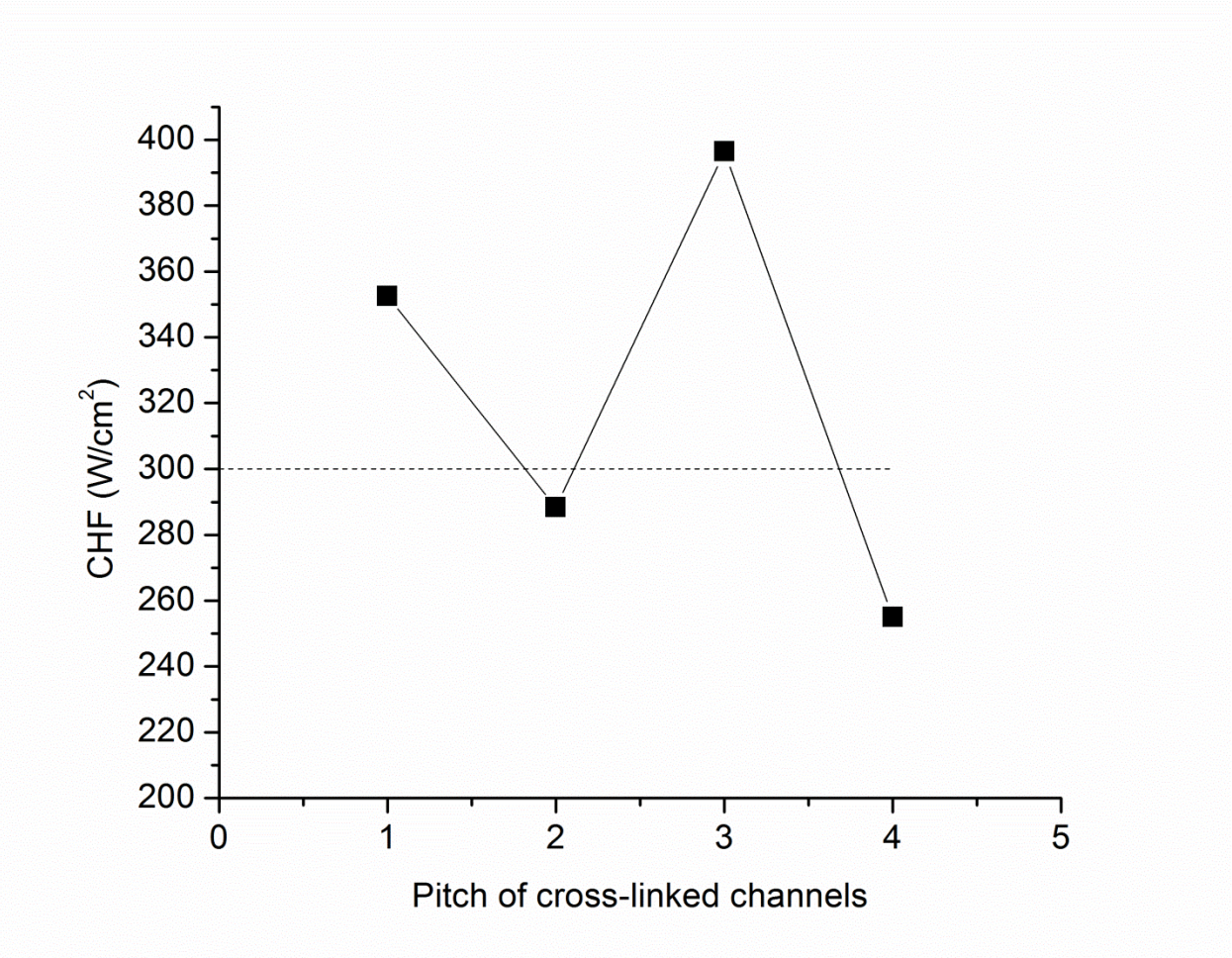

Figure 21: CHF trend in cross linked microchannel showing odd number of channels performing better than even number of channels

The temperature limit (85 °C) imposed for electronics cooling inhibits the use of water as a potential cooling fluid in these devices. Instead fluorient series fluids and refrigerants are suitable liquids due to their lower saturation temperatures. In this chapter, pool boiling tests of cross-linked surfaces with FC-87 at atmospheric conditions is presented. Specific details include experimental setup, test chips, results and discussions.

4.1 Experimental setup

Pool boiling performance of cross linked channels with FC-87 at atmospheric pressure was investigated. Experimental setup designed and fabricated by Kalani and Kandlikar [11] is used in this study. The main reason for using this setup stems from the fact that FC-87 has a relatively low boiling point (30 °C) and can evaporate at room temperature which required a chiller to condense the fluid. The setup consisted of a stainless steel cylindrical chamber (100 mm diameter) and a condensing unit. Fig. 20 shows the schematic of the experimental setup. C-clamps were used to seal the stainless steel chamber to the flanges on either ends. A see through glass window is provided on the walls of the cylindrical chamber on either side. The entire setup is made leak proof by sealing with O-rings wherever necessary.

The top flange is provided with openings for saturation thermocouple probe, FC-87 inlet port, vacuum port and inlet and outlet connections for copper condenser unit. A constant temperature circulating water bath provided necessary water flow at the desired temperature and flow rate to the condenser coil. A pressure gauge is mounted on the top flange to maintain the chamber at atmospheric conditions.

The bottom flange consisted of an opening for the heater assembly and auxiliary heater. The test chip was mounted on a garolite chip holder which was threaded to the bottom flange by means of four screws. The chip holder had 15 mm square opening to establish contact between the heater and the test chip. Grafoil was inserted to improve the contact. Garolite is selected due to low thermal conductivity (0.27 W/m K) and ability to withstand high temperatures (335 °F).

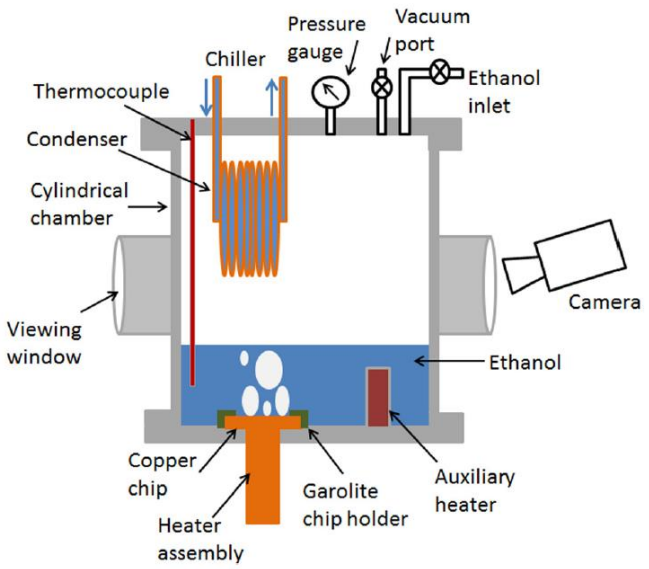

Figure 22. Pool boiling set up used by Kalani and Kandlikar [10] to test FC-87

4.2 Test chip

A test section similar to part-I is used. It consisted of 20 mm × 20 mm flat copper chip with 3 mm thickness with surface enhancement feature on a 10 mm × 10 mm area on the boiling surface. The heater side consisted of a 10 mm × 10 mm × 2 mm groove all around to reduce heat losses. A 0.7 mm hole was drilled to the center on one side of the test chip to accommodate the thermocouple for surface temperature measurement.

Heat flux was calculated using Eqn. (4) using three thermocouple measurements on the copper rod as shown in Fig. 22. One-dimensional conduction was established similar to part-I. The copper rod used for heating was wrapped with ceramic insulating sleeve to avoid heat losses and aid one-dimensional conduction.

A national instruments cDAQ-9172 data acquisition system was used to record temperature. The experimental procedure was similar to part-I.

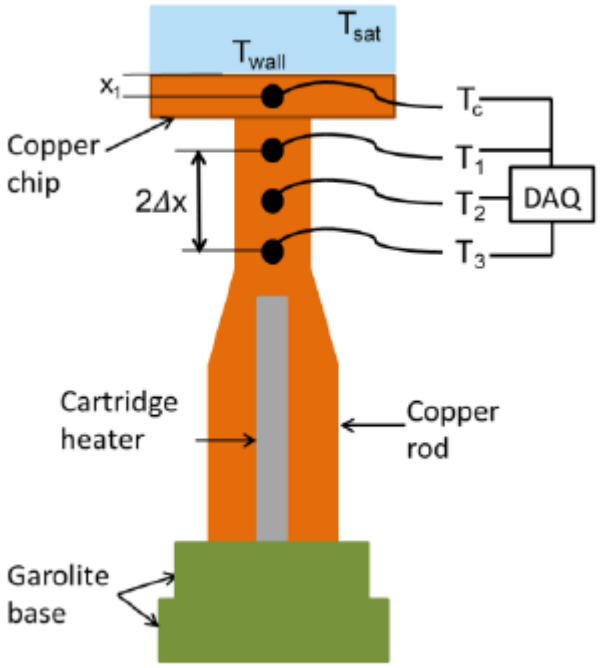

Figure 23. Schematic of heater assembly

4.3 Uncertainty analysis

An uncertainty analysis was conducted similar to chapter 2 and Ref. [11]. Thermocouple measurement was the main contributing factor to uncertainty. An uncertainty of 7% is observed at low heat flux values. As the heat flux is increased, which is the main region of interest in this study, the uncertainty drops to less than 5%.

4.4 Results

Fig. 23 shows the pool boiling curve for cross-linked microchannels with FC-87 at atmospheric pressure. Firstly, FC-87 is allowed to boil on a plain chip which is prepared by rubbing on 2000 grit sandpaper. A CHF of 10 W/cm^2 is observed and this will serve as baseline comparison for all enhancements reported in this study. A CHF of 16 W/cm^2, 17 W/cm^2, 20 W/cm^2 and 13 W/cm^2 is reported for 1, 2, 3 and 4 cross linked channels respectively. Large wall superheats are expected due to the poor thermal properties of fluorient fluids. The wall superheats are 30 °C, 46 °C, 35 °C, 40 °C and 27 °C for plain, 1, 2, 3 and 4 cross linked channels respectively. The cross linked chips show minimal enhancement at lower heat fluxes compared to a plain chip whereas at higher heat flux this enhancement is more pronounced. All tested chips follow similar pool boiling pattern in which natural convection is dominant in the initial phase till the onset of nucleate boiling where more nucleation sites become available which are responsible for increased heat dissipation rates. The experiments were stopped once CHF is attained which is seen by a sudden spike in the surface temperature indicating existence of a thin vapor blanket on the surface inhibiting heat transfer.

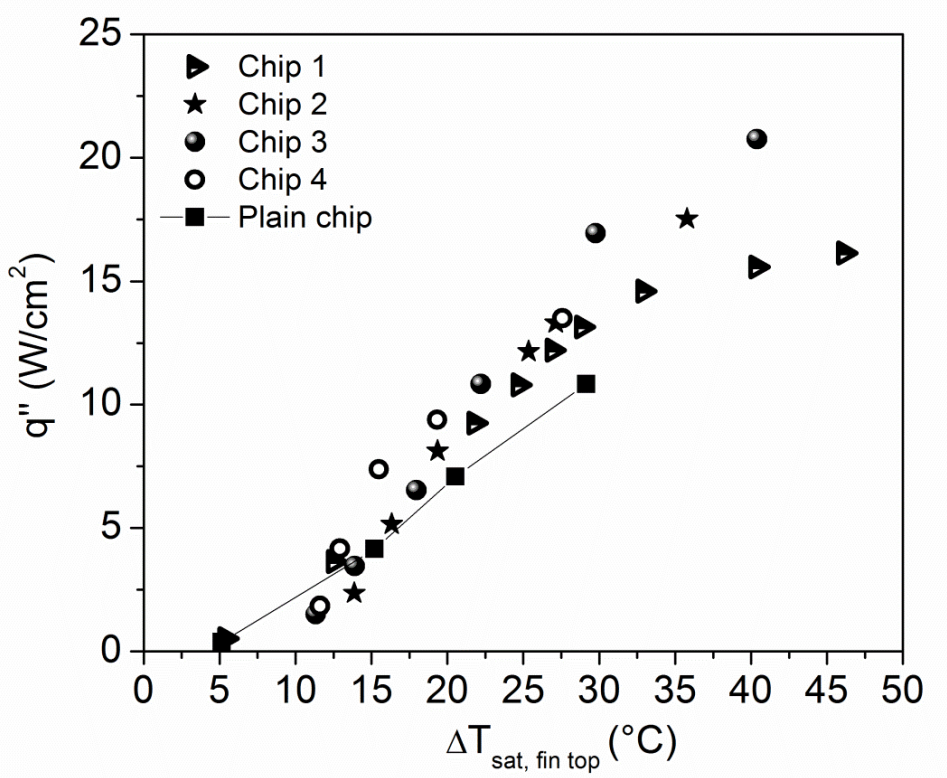

Figure 24. Pool boiling test results with FC-87 at atmospheric pressure

The trend observed overlays that depicted by water except for the microchannel with two cross-linked flow passages. Microchannel with three cross linked passages can be identified as the optimum geometry in this study to amplify performance in terms of CHF.

4.5 Comparison to literature

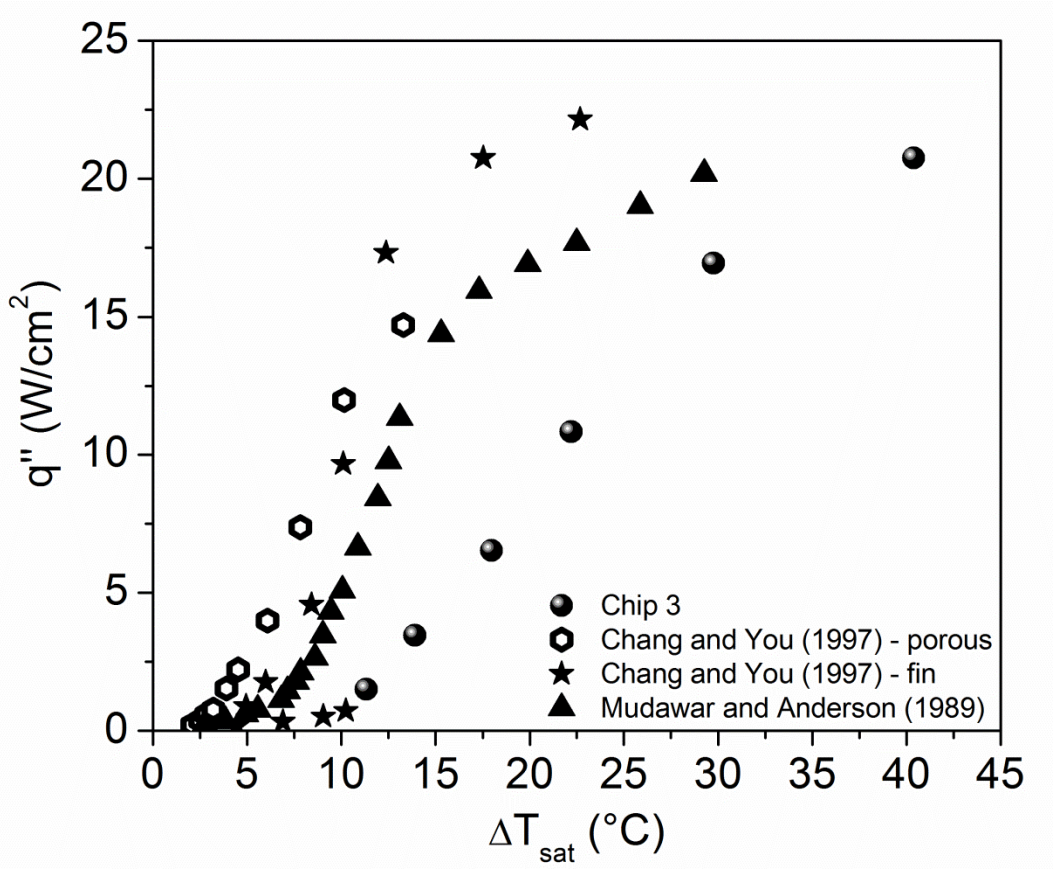

Figure 25. Pool boiling performance comparison with similar enhancements available in literature

Fig. 24 shows the pool boiling comparison with similar enhancement techniques available in literature. The best performing surface with 3 cross-linked flow passages underperforms when compared to other enhancement techniques reported here. However, the enhancement techniques correspond to tall fins in the order of 2 mm or more. It has been established in literature that tall fins due to additional surface area have shown significant enhancement. This study aims to improve the heat transfer performance with low fins in the order of 400 μm. At CHF, the best performing chip has a CHF of 21 W/cm^2 which is higher than that reported by Mudawar and Anderson [12]

and Chang and You [44]. Due to poor thermal properties of FC-87 high wall superheats are expected which is consistent with all the curves reported in this study.

4.6 Validation of mechanism

High speed images were inhibited by the design of the experimental setup used in this study. A similar trend is observed in CHF values when compared to water. The hypothesis can be validated by the similar trends observed.

Chapter 5

Chapter 3 and 4 describes the enhancement achieved from micromachined surfaces. The area enhanced surfaces also provide convective pathways for bubble removal and liquid recirculation. Also, literature review presented in chapter 1 has shown that porous surfaces provide additional nucleation sites which significantly reduce temperature difference and increase heat dissipation rates. Patil and Kandlikar [23] have shown that a combination of enhancement techniques results in high heat transfer coefficients. The scope of the current work is developed further by using sintering to create porous structures on open microchannel geometry. Furthermore, porous coatings are deposited on all microchannel regions in the boiling area, channel bottom and fin tops compared to Patil and Kandlikar [23] where deposition is reported only on microchannel fin tops. Open microchannel is selected as against cross-linked flow passages to establish that porous coatings can be deposited by sintering on these surfaces. Moreover, pool boiling performance on selectively sintered microchannels has never been done before which furthers strengthens the claim of the work presented in this chapter.

5.1 Experimental setup and data acquisition

Experiments were conducted with the same test setup reported in chapter 2. A National Instruments cDaq-9172 data acquisition system with NI-9213 temperature module was used to record the temperature. A LabVIEW VR virtual instrument displayed and calculated the surface temperature and heat flux.

5.2 Test chip

The test chips used were similar to that described in chapter 2. The enhancement on the 10 mm × 10 mm boiling surface is achieved by machining open microchannels with a channel width = 500 μm, fin width = 200 μm and fin depth = 400 μm. Porous coating is then deposited on this surface by screen printing using a powder to ink composition of 2:1. A commercially available copper powder from 3M™ with a particle size of 10 μm – 20 μm is used. Once porous coatings are deposited on the chip surface with the methods as described in the next paragraph, the test chips are subjected to sintering in an inert atmosphere. Sintering parameters for all test surfaces were maintained as shown in table 4.

Table 4. Sintering details used in this study

Parameter	Value
Sintering temperature	800 °C
Sintering duration	2 hours
Sintering atmosphere	Helium

Three surfaces were investigated in this study for its pool boiling performance with water as the working liquid at atmospheric pressure. For microchannel with porous fin tops, a two-step process is used where porous deposits are first screen printed (mesh size=230) on a plain chip and then microchannels are machined to achieve selective coating. For microchannels with deposits on the entire geometry a pass through a screen printing mesh (mesh size=230) is used and a coating thickness of roughly 100 μm is observed when measured under a laser confocal microscope. A similar approach for deposits on the channel bottom is obtained wherein after sintering; deposits on fin tops are removed by sanding on a 2000 grit sand paper.

Fig. 25 shows the scanning electron microscopy images of open microchannel selectively coated with porous deposits. The morphology obtained is moon-shaped morphology suggesting that screen printing with a mesh size of 230 and sintering with parameters mentioned in table 3 yields the above mentioned morphology. Since the same process is used in all tested surfaces the characterization of surfaces is uniform.

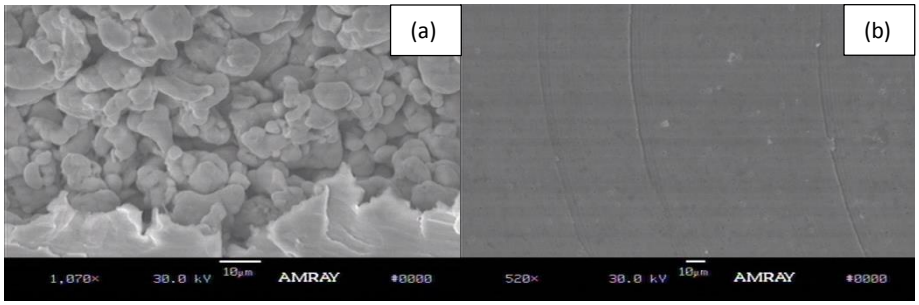

Figure 26. SEM images of sintered fin top surface (a) porous deposits obtained on sintered fin tops (b) no deposits in the channel

5.3 Results

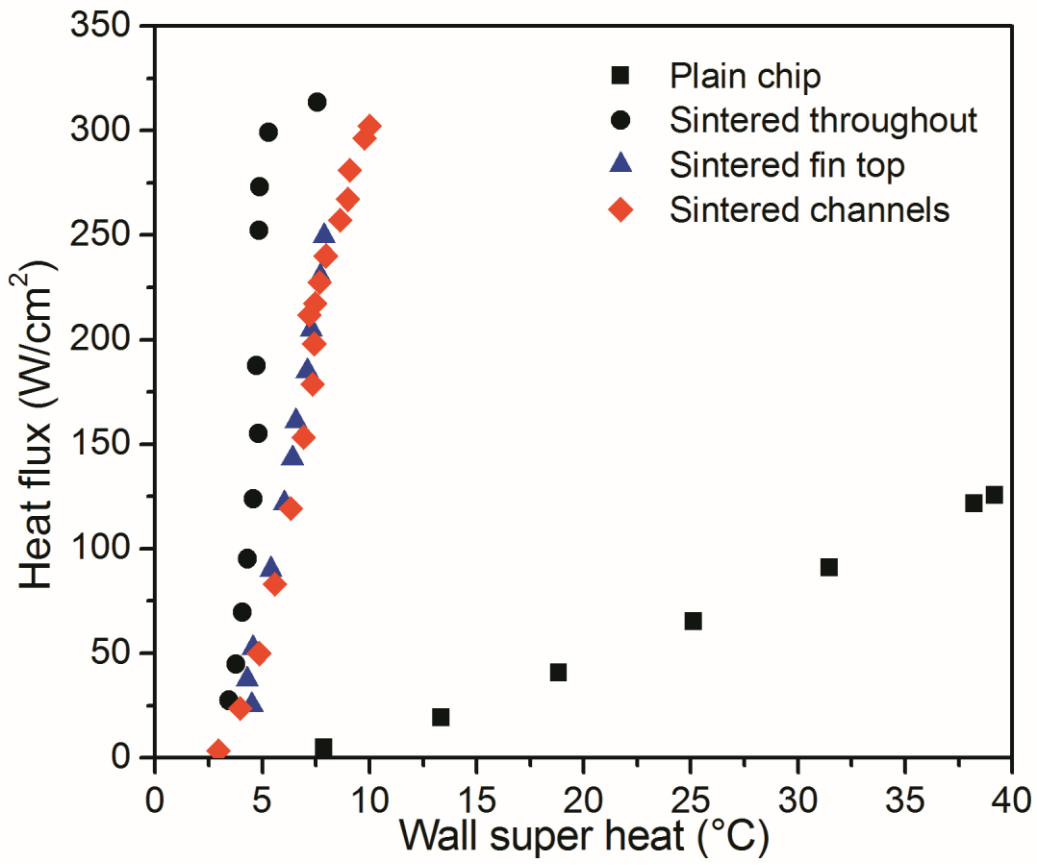

Figure 27. Pool boiling performance of porous sintered open microchannels with water at atmospheric conditions

Fig. 26 shows the pool boiling curve obtained for the three chips investigated in this study. To serve as a baseline for all enhancement comparisons, water is allowed to boil on a plain mirror finished copper. A CHF of 125 W/cm^2 is reported at a wall superheat of 40 °C. Pool boiling data for the three surfaces tested is reported in this curve. At lower heat fluxes all the test chips shows significant enhancement over a plain chip as seen by the steep slopes showing significant enhancement in heat transfer coefficients. At higher heat flux, the test chips with porous coatings throughout the open microchannel geometry perform slightly better than the other two surfaces. The best performing chip had a CHF of 313 W/cm^2 at a substantially low wall superheat of 7.5 °C. The chip with porous

coatings in the channel and on fin tops had a CHF of 302 W/cm^2 and 257 W/cm^2 at a wall superheat of 10 °C and 8.6 °C respectively. The chip with porous coating on the channel bottom had a better CHF value than the chip with porous fin tops which was contradictory to the study established by Patil and Kandlikar [23].

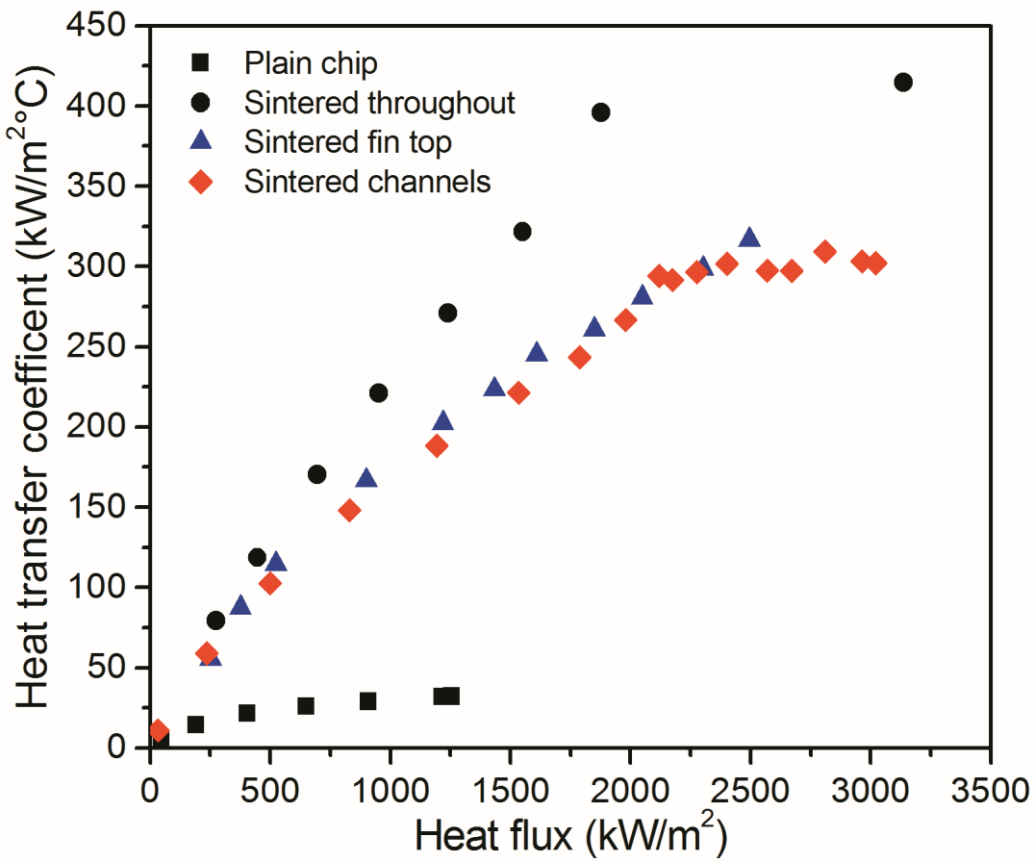

Figure 28. Heat transfer performance with water at atmospheric pressure

Fig. 27 shows the variation HTC plotted against the heat flux. It is evident that HTC increased with increasing heat fluxes although the last data marker for microchannel coated with porous coatings showed a significant dip which may be due to sudden overshoot in the temperature. The highest heat transfer coefficient reported in this study was 565 kW/m^2-°C representing an enhancement of 1800% compared to a plain chip. The general trend indicated high HTC values for all the tested surfaces. Chip with porous

fin tops and channel bottom had almost overlapping curves suggesting that some other mechanism may be responsible for the enhancement than that proposed by Patil and Kandlikar [23].

High speed images were taken to identify the location of bubble nucleation and observe any trend in bubble motion during its growth. Images reveal that nucleation occurs at the bottom of microchannels with porous coatings on the channel and fin tops. When the microchannel is entirely covered with porous coatings nucleation seems to occur at all locations. This observation contradicts the bubble nucleation phenomenon explained by Patil and Kandlikar [23] where bubbles were proposed to nucleate on microchannel porous fin tops. A different manufacturing technique to create porous coating could be the reason for the contradicting bubble behavior in open microchannels. However, additional nucleation sites provided by deposits on the entire microchannel geometry can be identified as the mechanism for CHF enhancement coupled with the high rewetting feature offered by open microchannels.

Bubble nucleation images

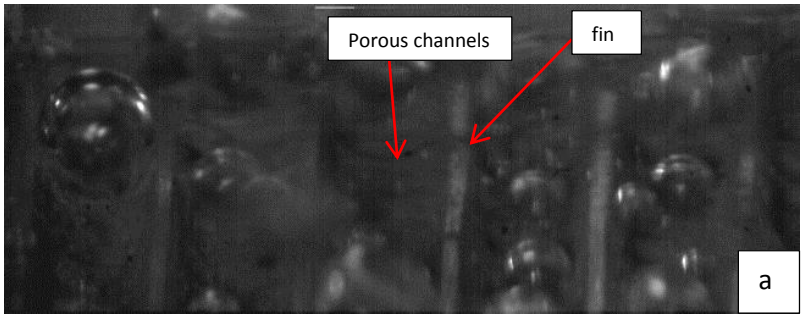

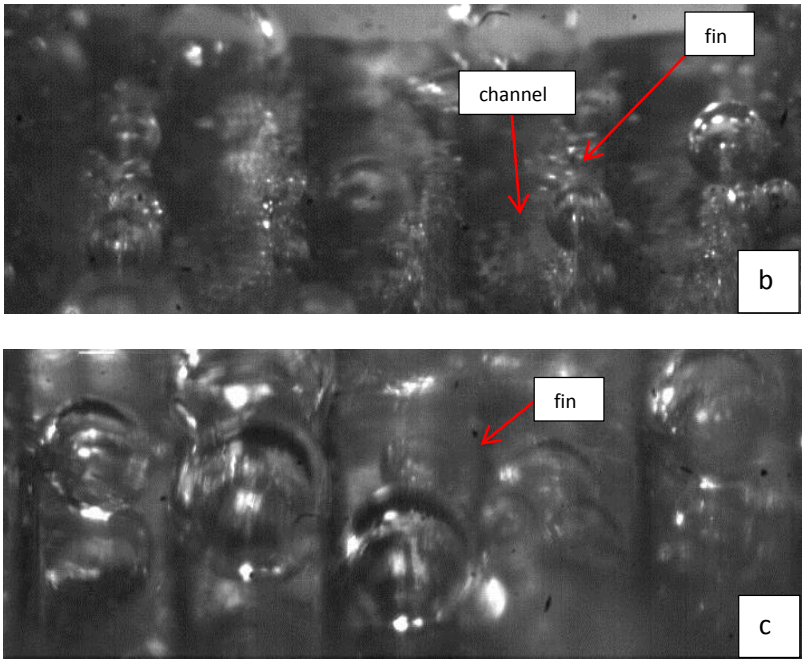

Figure 29. (a) Bubble nucleation in the channel bottom of porous sintered open microchannel (b) bubble nucleation on all locations of porous sintered open microchannel (c) bubble nucleation on channel bottom of porous sintered microchannel fin tops

Fig. 28 (a), (b) and (c) shows the location of bubble nucleation at low heat fluxes when porous coatings are sintered on channel bottom, fin tops, sidewalls and channel bottom and fin tops. From Fig. 28 (a) it is evident that bubbles nucleate only on channel bottom and no bubbles are seen on fin tops whereas Fig 28 (b) with porous coatings throughout the geometry indicate bubble nucleation in the channel bottom, sidewalls and fin tops. Additional nucleation sites can be identified as the main reason for more bubbles to nucleate. For microchannel with porous fin tops, bubbles seem to nucleate only in the channel bottom.

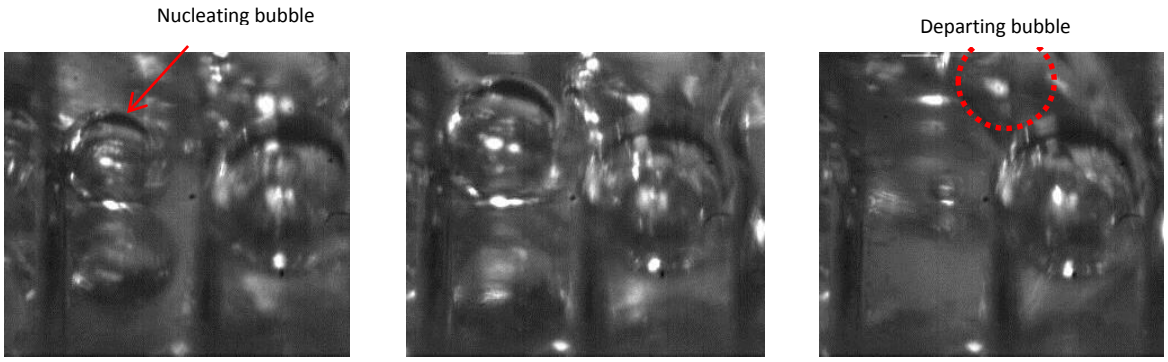

Figure 30. Bubble growth in the channels of porous microchannel fin tops

Bubble growth mechanism indicates identical mechanism described in chapter 2. For bubble growth in the channels, bubbles nucleate in the channel bottom successively growing to the channel width from where it departs into the bulk liquid. This mechanism is consistent with open microchannel enhancement as seen with cross-linked flow and porous coatings on microchannels as shown in Fig. 29.

5.4 Comparison to literature

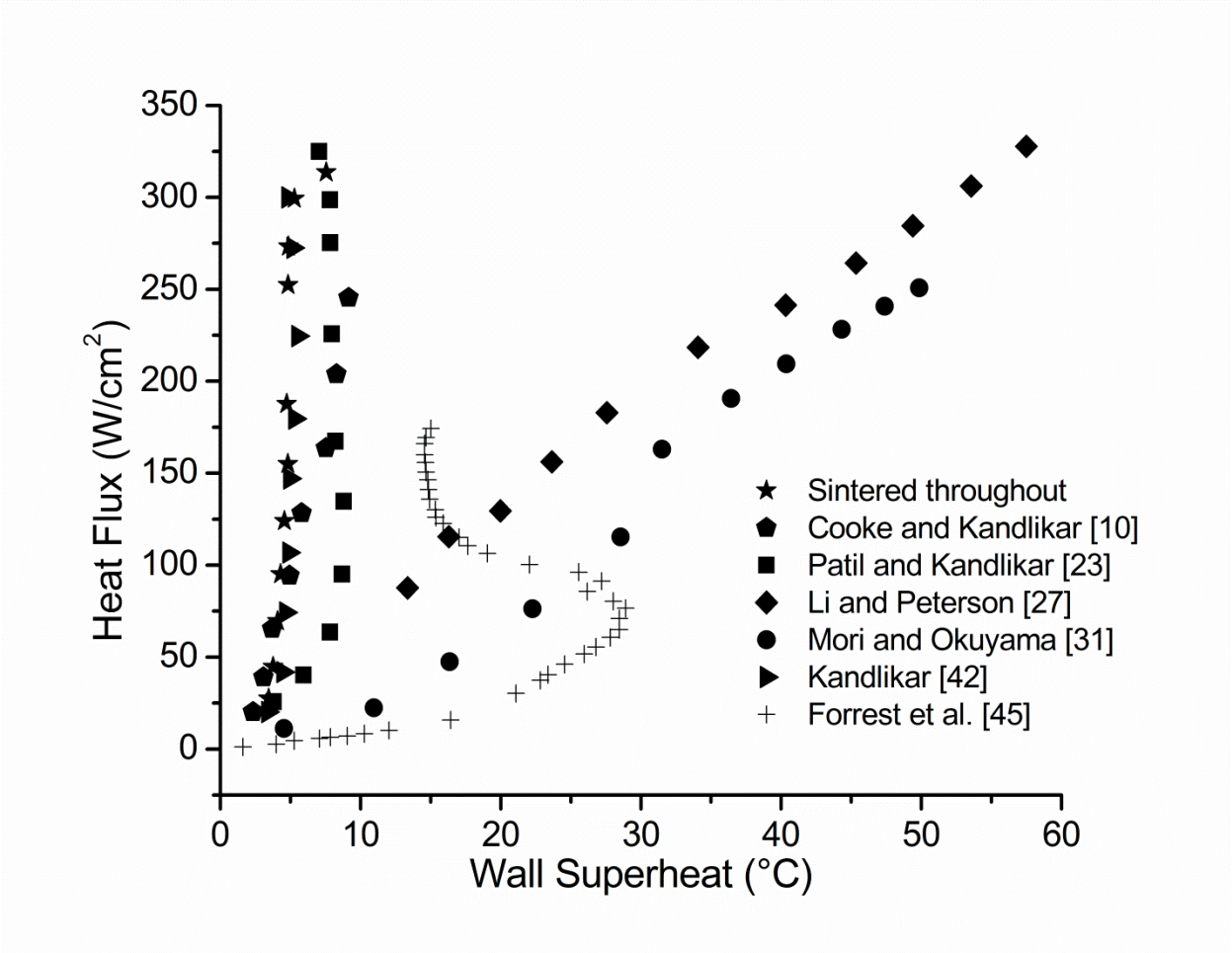

Figure 31. Pool boiling comparison curves for surface completely covered with porous deposits in this study with results available in literature [10, 23, 27, 31, 42, 45]

Pool boiling comparison was drawn with the highest performing chip in this study with that available [10,23,27,31,42,45] and is presented in Fig. 30. The CHF value is in close comparison with that reported by Kandlikar [42] and Patil and Kandlikar [23]. Mori and Okayuma [31] and Li and Peterson [46] have reported higher CHF values however, their wall superheats are in excess of 50 °C which is undesirable. The wall superheat observed in this study is 7.5 °C. A CHF of 313 W/cm^2 is observed in this study. The path traced by this curve overlay that reported by Patil and Kandlikar [23] although selective coating may not necessarily have improved the CHF

as reported by them. Furthermore, a different bubble growth and departure cycle is observed which could be the underlying reason for the above statement.

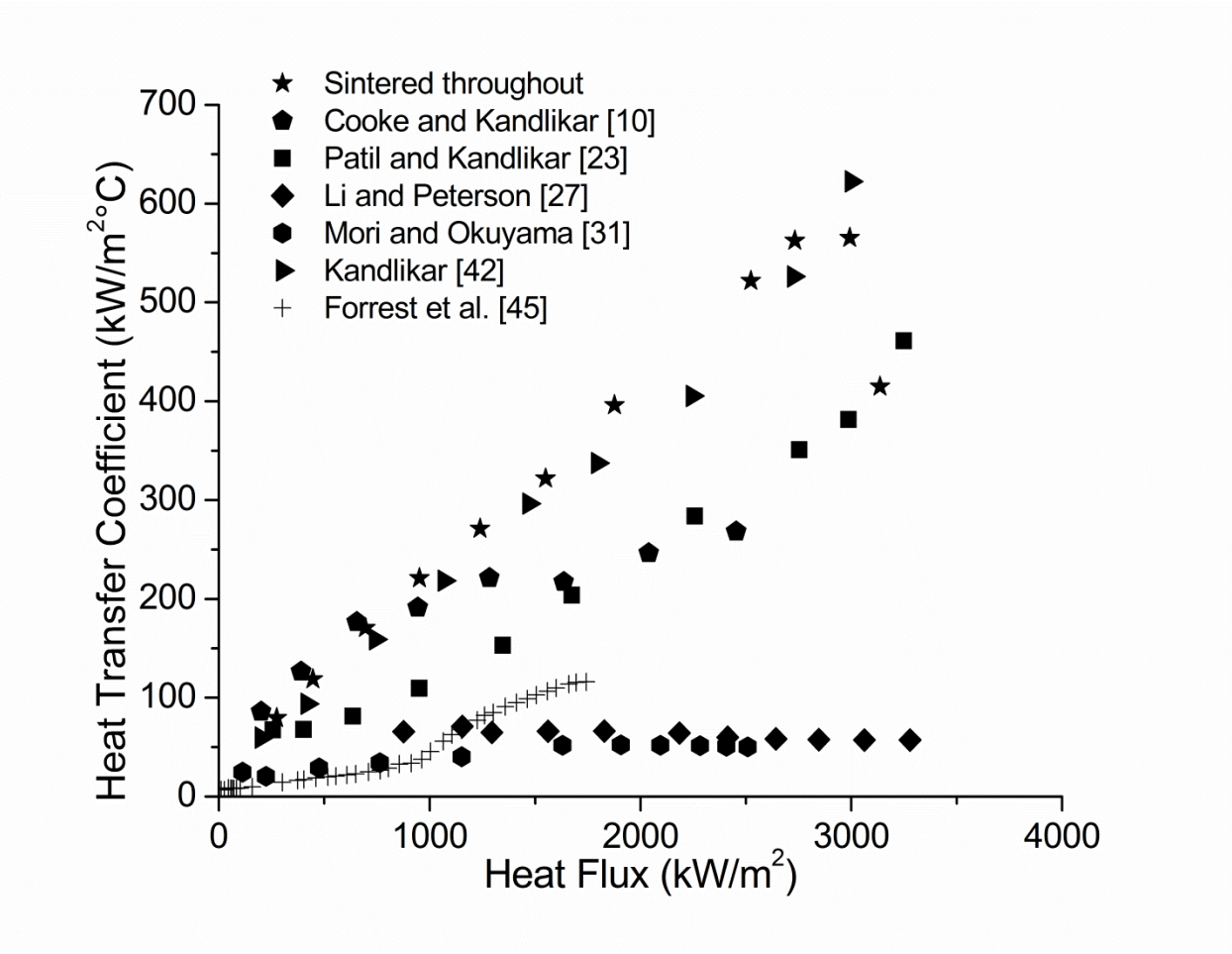

Figure 32. Heat transfer coefficient for completely sintered surface with results from literature [10, 23, 27, 31, 42, 45]

Fig. 31 represents comparison of heat transfer coefficient obtained in this study with that available in literature. A close comparison can be drawn with the best performing chip and record heat transfer coefficient reported by Kandlikar [42] based on evaporation momentum force. Also, this surface performs slightly better than Patil and Kandlikar [23] at points leading to CHF.

6.1 Conclusions

In this thesis, a two part study was conducted to develop heat transfer surface enhancement over open microchannel surface. In part-I of this study, effect of channel pitch of cross-linked surfaces was investigated. The surface was fabricated by micromachining making it very convenient to fabricate. The following key points are drawn from Part-I of this study,

1. Micromachining technique was used to develop a heat transfer surface using CNC machine.
2. Four test surfaces were prepared to study the effect of cross-linked channel pitch on its pool boiling performance.
3. The resulting surface is tested for its pool boiling performance with water and FC-87. The best performing chip with three cross-linked flow passages yielded a CHF of 396 W/cm^2 with water at a wall superheat of 7.3 °C and had a 167% enhancement in CHF compared to a plain chip. Test chip with one cross-linked passage had a CHF of 352 W/cm^2 at a wall superheat of 14 °C. Tests chips with two and four cross-linked passages had a CHF of 288 W/cm^2 and 255 W/cm^2 respectively. All the chips investigated in this study had a significant improvement in CHF over an open microchannel without cross-linked flow suggesting that cross-linked flow performed better than open microchannels.

4. When tested with FC-87, CHF of 21 W/cm^2 is reported for microchannel with three cross linked passages which had an enhancement of 110% in CHF when compared to a plain chip.
5. CHF trend is identified which shows that cross-linked flow with odd number of passages performed better than even number of passages. The CHF trend observed with water overlays that with FC-87 except for microchannel with two cross-linked passages.
6. High speed imaging suggests that bubble nucleation occurs at the bottom corner of the channels from where they grow to the channel width and rise to the fin top. Bubble departure takes place from fin tops without any observable pinning.

In part-II of the study, heat transfer surface was developed by selectively coating porous particles on open microchannel fin tops, channels and entire geometry. Sintering at elevated temperatures ensured good substrate bonding. Following key points can be drawn from this study,

1. A heat transfer surface was developed by screen printing on open microchannel geometry. Three surfaces were fabricated by depositing on fin tops, channel bottom and throughout the geometry.
2. A CHF of 313 W/cm^2 is observed at a wall superheat of 7.5 °C for the chip completely covered with porous deposits. Substrate bonding was achieved by sintering at elevated temperatures in an inert atmosphere. CHF of 303 W/cm^2 and 257 W/cm^2 is reported for microchannel with porous deposits in the channel and on fin tops respectively.

3. Bubble dynamics supported by high speed imaging suggests that bubble nucleation takes place at locations of porous deposits except for microchannel with porous fin tops were nucleation occurs at the bottom.
4. Additional nucleation sites provided by porous deposits and superior irrigation pathways and liquid recirculation provided by open microchannels can be attributed to the enhancement provided by this surface.

6.2 Recommendations for future work

The cross-linked flow can be enhanced further by depositing porous coatings. Porous coatings, as suggested by part-II of the study provide high heat dissipation rates at considerably low wall superheats.

Graphene and nanowires have garnered keen attention of researchers due to its excellent thermal and liquid wetting properties respectively. Cross-linked and porous microchannel surfaces can be enhanced further by coating graphene or growing nanowires to further augment the pool boiling surface.

To improve performance of cross-linked flow with FC-87 tall fins can be provided and heat flux in the range of 100 W/cm^2 can be achieved. The study can be extended to potential fluids like binary mixtures, nanofluids and R-134a.

6.3 References

[1] D. BTuckerman, D. B., and Pease, R. F. W., "High-performance heat sinking for VLSI," Electron Device Lett IEEE, **2**(5), pp. 126–129.

[2] Hsu, Y. Y., and Graham, R. W., 1961, "Analytical and experimental study of thermal boundary layer and ebullition cycle in nucleate boiling," Natl. Aeronaut. Space Adm. -- Tech. Notes, p. 43.

[3] Hsu, Y. Y., 1961, "On size range of active nucleation cavities on heating surface," ASME Meeting WA-177, Nov 26-Dec 1 1961, American Society of Mechanical Engineers (ASME), p. 7.

[4] Kandlikar, S. G., and Spiesman, P. H., 1998, "Effect of surface finish on flow boiling heat transfer," Proceedings of the 1998 ASME International Mechanical Engineering Congress and Exposition, November 15, 1998 - November 20, 1998, ASME, pp. 157–163.

[5] Kandlikar, S. G., Shoji, M., and Dhir, V. K., 1999, Handbook of Phase Change: Boiling and Condensation, Taylor & Francis.

[6] Nukiyama, S., 1934, "Maximum and minimum values of heat transmitted from metal to boiling water under atmospheric pressure," Soc. Mech. Eng. Jpn. -- J., **37**(206), pp. 367–374.

[7] Bui, T. D., and Dhir, V. K., 1985, "Transition boiling heat transfer on a vertical surface," Trans. ASME J. Heat Transf., **107**(4), pp. 756–63.

[8] Marto, P. J., and Rohsenow, W. M., 1966, The effect of surface conditions on nuceate pool boiling heat transfer to sodium, Cambridge, Mass. : M.I.T. Dept. of Mechanical Engineering, [1965].

[9] Mehta, J. S., and Kandlikar, S. G., 2013, "Pool boiling heat transfer enhancement over cylindrical tubes with water at atmospheric pressure, Part I: Experimental results for circumferential rectangular open microchannels."

[10] Cooke, D., and Kandlikar, S. G., 2012, "Effect of open microchannel geometry on pool boiling enhancement," Int. J. Heat Mass Transf., **55**(4), pp. 1004–1013.

[11] Kalani, A., 2012, "Experimental Investigation of Pool Boiling Performance with Ethanol and FC-87 on Open Microchannel Surfaces," Master's, Rochester Institute of Technology.

[12] Mudawar, I., and Anderson, T. M., "Microelectronic Cooling by Enhanced Pool Boiling of a Dielectric Fluorocarbon Liquid," Trans. ASME, **111**, pp. 752–759.

[13] Cora, Ö. N., Min, D., Koç, M., and Kaviany, M., 2010, "Microscale-modulated porous coatings: fabrication and pool-boiling heat transfer performance," J. Micromechanics Microengineering, **20**(3), p. 035020.

[14] Hanlon, M. A., and Ma, H. B., 2012, "Evaporation heat transfer in sintered porous media," J. Heat Transf., **125**(4), pp. 644–652.

[15] Saeidi, D., and Alemrajabi, A. A., 2013, "Experimental investigation of pool boiling heat transfer and critical heat flux of nanostructured surfaces," Int. J. Heat Mass Transf., **60**(1), pp. 440–449.

[16] Yao, Z., Lu, Y.-W., and Kandlikar, S. G., 2012, "Pool boiling heat transfer enhancement through nanostructures on silicon microchannels," J. Nanotechnol. Eng. Med., **3**(3).

[17] Sathyamurthi, V., and Banerjee, D., 2010, "Dynamics of pool boiling on plain and nanotube coated silicon surfaces," 2010 14th International Heat Transfer

Conference, IHTC 14, August 8, 2010 - August 13, 2010, American Society of Mechanical Engineers, pp. 563–576.

[18] You, S. M., Kim, J. H., and Kim, K. H., 2003, "Effect of nanoparticles on critical heat flux of water in pool boiling heat transfer," Appl. Phys. Lett., **83**(16), pp. 3374 –3376.

[19] Hai Trieu Phan, Caney, N., Marty, P., Colasson, S., and Gavillet, J., 2011, "Enhancement of flow boiling heat transfer in microchannels by nanoand micro-surface treatments," Mec. Ind., **12**(3), pp. 151–5.

[20] Wen, D., and Ding, Y., 2005, "Experimental investigation into the pool boiling heat transfer of aqueous based γ-alumina nanofluids," J. Nanoparticle Res., **7**(2-3), pp. 265–274.

[21] Patil, C. M., and Kandlikar, S. G., "Review of the Manufacturing Techniques for Porous Surfaces Used in Enhanced Pool Boiling," Heat Transf. Eng., **0**(ja), p. null.

[22] Patil, C. M., Santhanam, K. S. V., and Kandlikar, S. G., 2014, "Development of a two-step electrodeposition process for enhancing pool boiling," Int. J. Heat Mass Transf., **79**, pp. 989–1001.

[23] Patil, C. M., and Kandlikar, S. G., 2014, "Pool boiling enhancement through microporous coatings selectively electrodeposited on fin tops of open microchannels," Int. J. Heat Mass Transf., **79**, pp. 816–828.

[24] Patil, C. M., Kandlikar, S. ., and Santhanam, K. S. ., "Development of a two-step electrodeposition process for enhancing pool boiling," Int. J. Heat Mass Transf.

[25] Patil, C. M., and Kandlikar, S. ., "Pool boiling enhancement through microporous coatings selectively electrodeposited on fin tops of open microchannels," Int. J. Heat Mass Transf.

[26] Nakayama, W., Daikoku, T., and Nakajima, T., 1982, "Effects of Pore Diameters and System Pressure on Saturated Pool Nucleate Boiling Heat Transfer from Porous Surfaces," J Heat Transf. U. S., **104:2**.

[27] Li, C., and Peterson, G. P., 2007, "Parametric study of pool boiling on horizontal highly conductive microporous coated surfaces," J. Heat Transf.-Trans. Asme, **129**(11), pp. 1465–1475.

[28] WEBB, R. L., 1981, "Nucleate Boiling on Porous Coated Surfaces," Heat Transf. Eng., **4**(3-4), pp. 71–82.

[29] Afgan, N., Stefanovic, M., Jovanovic, L., and Pislar, V., 1973, "Determination of the statistical characteristics of temperature fluctuation in pool boiling," Int. J. Heat Mass Transf., **16**(2), pp. 249–56.

[30] A.E.Bergles, and M.C.Chyu, 1982, "Characteristics of Nucleate Pool Boiling From Porous Metallic Coatings," J. Heat Transf., **104**, pp. 279–285.

[31] Mori, S., and Okuyama, K., 2009, "Enhancement of the critical heat flux in saturated pool boiling using honeycomb porous media," Int. J. Multiph. Flow, **35**(10), pp. 946–951.

[32] Ahn, H. S., Lee, C., Kim, J., and Kim, M. H., 2012, "The effect of capillary wicking action of micro/nano structures on pool boiling critical heat flux," Int. J. Heat Mass Transf., **55**(1–3), pp. 89–92.

[33] Sato, T., Ohtake, H., and Koizumi, Y., 2009, "Experimental study on nucleation site interaction during pool nucleate boiling by using three artificial cavities," 2008 ASME International Mechanical Engineering Congress and Exposition, IMECE 2008, October 31, 2008 - November 6, 2008, American Society of Mechanical Engineers, pp. 901–905.

[34] Honda, H., and Wei, J. J., 2004, "Enhanced boiling heat transfer from electronic components by use of surface microstructures," Exp. Therm. Fluid Sci., **28**(2–3), pp. 159–169.

[35] Arik, M., Bar-Cohen, A., and You, S. M., 2007, "Enhancement of pool boiling critical heat flux in dielectric liquids by microporous coatings," Int. J. Heat Mass Transf., **50**(5-6), pp. 997–1009.

[36] Kim, J. H., Kwark, S. M., Kashinath, M. R., and You, S. M., 2007, "Optimization of microporous structures in enhancing pool boiling heat transfer of saturated R-123, FC-72 and water," 2007 ASME/JSME Thermal Engineering Summer Heat Transfer Conference, HT 2007, July 8, 2007 - July 12, 2007, American Society of Mechanical Engineers, pp. 349–356.

[37] Hegde, R. N., Rao, S. S., and Reddy, R. P., 2012, "Investigations on boiling-induced nanoparticle coating, transient characteristics, and effect of pressure in pool boiling heat transfer on a cylindrical surface," Exp. Heat Transf., **25**(4), pp. 323–40.

[38] Pastuszko, R., and Piasecka, M., 2012, "Pool boiling on surfaces with mini-fins and micro-cavities," 6th Eur. Therm. Sci. Conf. Eurotherm 2012, **395**, p. 012137.

[39] Pastuszko, R., 2013, "Pool boiling on rectangular fins with tunnel-pore structure," Efm12 - Exp. Fluid Mech. 2012, **45**.

[40] Rainey, K. N., You, S. M., and Lee, S., 2003, "Effect of pressure, subcooling, and dissolved gas on pool boiling heat transfer from microporous, square pin-finned surfaces in FC-72," Int. J. Heat Mass Transf., **46**(1), pp. 23–35.

[41] Guglielmini, G., Misale, M., and Schenone, C., 2002, "Boiling of saturated FC-72 on square pin fin arrays," Int. J. Therm. Sci., **41**(7), pp. 599–608.

[42] Kandlikar, S. G., 2013, "Controlling bubble motion over heated surface through evaporation momentum force to enhance pool boiling heat transfer," Appl. Phys. Lett., **102**(5), p. 051611.

[43] Kalani, A., and Kandlikar, S. G., 2014, "Evaluation of pressure drop performance during enhanced flow boiling in open microchannels with tapered manifolds," J. Heat Transf., **136**(5).

[44] Chang, J. Y., and You, S. M., 1997, "Enhanced boiling heat transfer from microporous surfaces: effects of a coating composition and method," Int. J. Heat Mass Transf., **40**(18), pp. 4449–4460.

[45] Forrest, E., Williamson, E., Buongiorno, J., Hu, L.-W., Rubner, M., and Cohen, R., 2010, "Augmentation of nucleate boiling heat transfer and critical heat flux using nanoparticle thin-film coatings," Int. J. Heat Mass Transf., **53**(1–3), pp. 58–67.

[46] Hailei Wang, and Peterson, R. B., 2010, "Enhanced Boiling Heat Transfer in Parallel Microchannels With Diffusion Brazed Wire Mesh," IEEE Trans. Compon. Packag. Technol., **33**(4), pp. 784–93.